UNIVERSITY OF MISKOLC
FACULTY OF MECHANICAL ENGINEERING AND INFORMATICS

CHARACTERIZATION OF FLUID FLOW PROPERTIES OF NANOFLUIDS IN A PIPE

PHD THESES

Prepared by

Mohsen Khalili Najafabadi
Engineering of Chemical Engineering (BSc),
Engineering of Petroleum Engineering (BSc),
Engineering of Chemical Engineering (MSc)

ISTVÁN SÁLYI DOCTORAL SCHOOL OF MECHANICAL ENGINEERING SCIENCES
TOPIC FIELD OF MECHANICAL ENGINEERING SCIENCES
TOPIC GROUP OF DESIGN OF MACHINES AND ELEMENTS

Head of Doctoral School

Dr. Gabriella Bognár
DSc, Full Professor

Head of Topic Group

Dr. Gabriella Bognár

Scientific Supervisors

Dr. Gabriella Bognár
Dr. Krisztián Hriczó

Miskolc
2024

CONTENTS

SUPERVISOR'S RECOMMENDATIONS

Date

Supervisor

LIST OF SYMBOLS AND ABBREVIATIONS

Nomenclature

C_p	Constant-pressure specific heat, J/kgK
D_{in}	Inner diameter, m
f	Friction factor
C_f	Skin friction coefficient
Gz	Graetz number
h	Heat transfer coefficient, W/m^2K
k	Thermal conductivity, W/mK
L	Length, m
r	radial axis, m
R	Radius of the pipe, m
X_{hy}	Hydrodynamic entry length, m
X_{th}	Thermal entry length, m
$\dot{m}$	Mass flow rate, kg/s
Nu	Nusselt number
P	Pressure, Pa
Pr	Prandtl number
q	Heat transfer rate, W
q''	Surface heat flux, W/m^2
Re	Reynolds number
T	Temperature, K
x	Distance from inlet, m
x^*	Non-dimensional axial distance
$\vec{V}$	Velocity vector (u,v)
τ	Shear stress, Pa
$\dot{W}$	Pumping power, W
$\dot{V}$	Volume flow rate, m^3/s

Abbreviations

Exp	Experimental
CFD	Computational Fluid Dynamics
PEI	Performance Efficiency Index

Greek letters

β	Constant
ρ	Density, kg/m^3
φ	Nanoparticle volume fraction
μ	Viscosity, kg/ms

Subscripts

nf	Nanofluid
mnf	Mono nanofluid
hnf	Hybrid nanofluid
np	Nanoparticle
bf	Base fluid
b	Bulk
in	Inlet
out	Outlet
m	Mean
avg	Average
w	Wall

1. INTRODUCTION

Efforts to improve the heat transfer properties of coolants have been ongoing for decades. Advances in materials science and manufacturing technologies have allowed researchers to investigate the suspension of nanoscale particles in coolants, leading to the emergence of nanofluids. Choi et al. [1] are pioneers of this technique and their work has shown significant improvements in the thermal conductivity of the working fluid. The thermal conductivity of the working fluid is of paramount importance in the design of heat transfer devices. However, cooling capabilities were limited due to the low thermal conductivity of conventional working fluids used in heat transfer. Convective heat transfer occurs at the surface of particles. Therefore, the large surface area of nanoparticles has been shown to be suitable for increasing heat transfer capabilities. Particles with nanometre size enhance the thermal conductivity of the fluid rather than restricting the flow paths. Das et al. [2] conducted experiments to investigate how nanoparticles affect the thermal conductivity of nanofluids. They found a threefold improvement in the thermal conductivity of the working fluids.

The thermophysical properties of fluids can be significantly altered by the introduction of nanoparticles into the working fluid [3]. For example, the thermal entry length can change depending on whether the thermal conductivity of the nanofluid is higher or lower than that of the starting working fluid. The thermal entry length may be shorter due to more efficient heat transfer if the thermal conductivity is higher than that of the starting working fluid. Conversely, if the thermal conductivity is poor, heat transfer may be less efficient, resulting in a longer thermal entry length [4]. The incorporation of nanoparticles can further modify the velocity and temperature profiles near the pipe wall, further affecting the thermal entry length. Therefore, the specific properties of the nanofluid must be carefully considered when predicting the thermal entry length.

Authors studying the impact of using nanoparticles for heat transfer enhancement consider both laminar and turbulent flow conditions, depending on their research objectives. Laminar flows are often preferred for simplified modelling and theoretical analysis, allowing for a fundamental understanding of heat transfer mechanisms. However, many researchers also investigate turbulent flows, which are more representative of practical engineering applications, to provide a comprehensive understanding of nanofluid effects across different flow conditions.

Yang and his co-workers [5] conducted experiments on the laminar flow of water-based graphite fluid and observed an improvement in convective heat transfer. Their results showed that the heat transfer coefficient showed an increasing trend with Reynolds number and nanoparticle concentration, while a decrease was observed with decreasing fluid temperature.

With exceptional thermal properties, Al_2O_3-based nanofluids have a wide range of applications in heat exchangers, cooling systems, electronics, and automotive industries. Among the various nanofluids, Al_2O_3-based nanofluids have received considerable attention and applications in solar collectors. Non-metallic nanofluids have shown a higher potential to improve the efficiency of solar collectors compared to metal-based nanofluids [6]. Mahian et al. [7] evaluated the performance of a mini-channel solar collector by incorporating various metal and metal oxide nanoparticles. The results showed that Al_2O_3 exhibited the highest heat transfer coefficient among the nanoparticles investigated, ahead of Cu, SiO_2 and TiO_2. Hwang et al. [8] investigated the fully developed laminar flow of Al_2O_3-water nanofluid in a uniformly heated circular tube. The results revealed that employing Al_2O_3-water nanofluids with a concentration of 0.3 vol% resulted in an 8% enhancement in the heat transfer coefficient, surpassing the performance of a pure fluid.

In [9], it was demonstrated that Al_2O_3-water nanofluids outperform multi wall carbon nanotubes (MWCNT)-water nanofluids in terms of heat transfer, primarily due to the relatively lower viscosity of Al_2O_3-water nanofluids. Alim et al. [10] investigated the impact of suspended nanoparticles (specifically, Al_2O_3 dispersed in water) at different volume fractions ranging from 1% to 4% on heat transfer enhancement in an absorbing medium within a flat plate solar collector. The study demonstrated a substantial improvement in convective heat transfer with the inclusion of nanoparticles in the base fluid. Yousefi et al. [11] examined the impact of using Al_2O_3-water nanofluid as the working fluid on the efficiency of a flat-plate solar collector. The results revealed that compared to using water alone as the working medium, incorporating nanofluids resulted in a significant 28.3% improvement in efficiency when using a concentration of 0.2 wt% nanoparticles in the base fluid.

Engine oils are widely used as thermal fluids in many heat transfer applications where high temperatures present a challenge and water-based nanofluids prove inadequate, such as in the car industry [12]. Dispersing nanoparticles into engine oils can enhance both the cooling and lubrication performance to an even greater extent [13]. Many considerations must be taken into account when choosing an engine oil for heat transfer purposes because engine oils differ in terms of thermal conductivity, viscosity, temperature conditions, pour point, and so on. The use of engine oils with lower viscosity in engines, for instance, results in reduced pressure loss, whereas increased thermal conductivity results in improved heat transfer performance. Employing the appropriate engine oil could result in improved engine performance. However, relatively few studies have been carried out in this area [14–17].

Studies have revealed that hybrid nanofluids exhibit higher heat transfer efficiency compared to traditional fluids that contain only one type of nanoparticle [18]. As per published research, the use of a hybrid nanofluid can be substituted by a mono nanofluid as it enhances the rate of heat transfer [19,20]. More experimental study, however, is required to solve several issues associated to hybrid nanofluids, including skin friction coefficient increase, instability, and cost of preparation [18]. The improved performance was linked to a larger Nusselt number, which may be boosted by using hybrid nanofluids [21,22]. Unfortunately, no universal results have been reached on which nanofluids, mono or hybrid, provide the best performance [23]. The impact of the concentration of nanoparticles on the dynamic viscosity of Al_2O_3-oil was investigated by Hemmat et al. [24]. Their findings revealed that viscosity shows an increasing trend with increasing nanoparticle volume fraction. Another study [25] investigated the CuO-oil nanofluid at different nanoparticle weight fractions ranging from 0.2% to 2%. The findings indicated that the samples exhibited Newtonian behavior in the examined concentration range. Farbod et al. [26] investigated the CuO-oil nanofluid at a broad range of nanoparticle weight concentrations from 0.2% to 6%. They found that the nanofluid displayed Newtonian behavior. Asadi et al. [12] studied the use of MWCNT:Al_2O_3-oil hybrid nanofluid as a heat transfer fluid. Their results showed some positive effects on heat transfer performance in an internal laminar flow. In other investigations [27,28], the Nusselt number of a Cu:Al_2O_3-water hybrid nanofluid was found to be significantly greater than that of an Al_2O_3-water mono nanofluid.

Kumar et al. [29] compared the thermal performance and friction for turbulent flow of Al_2O_3-water nanofluid and Al_2O_3:CuO-water hybrid nanofluid. It was concluded that the hybrid nanofluid showed higher thermal performance values compared to Al_2O_3-water. Furthermore, experimental and numerical results were obtained for different concentrations of fly ash nanofluid [30,31] and fly ash:Cu hybrid water-based nanofluid turbulent flows. For a 2% volume fraction concentration, a very significant increase in performance efficiency.

The hydrodynamic and thermal entry lengths of a pipe flow are the distances required for the flow velocity to reach fully developed region and the temperature profile to become uniform. These entry lengths play a pivotal role in understanding flow and heat transfer characteristics. For design engineers, specifically, their determination is crucial as it reveals the relationship between the velocity profile, heat transfer coefficients and axial position. In addition to the critical investigation of the effect of nanoparticle volume fraction on hydrodynamic and thermal entry lengths, the selection of alumina (Al_2O_3) nanofluids is driven by their widespread relevance and applicability in various industrial and engineering contexts. Alumina nanoparticles are known for their stability, thermal conductivity, and chemical inertness, making them a prominent choice for enhancing heat transfer in diverse systems. The focus on Al_2O_3 nanofluids not only addresses fundamental questions about flow and heat transfer but also aligns with the practical significance of alumina nanoparticles in potential technological applications, for instance, heat exchangers, oil engines, solar collectors, and so forth, ensuring the broader implications of my research findings.

These measurements help to determine whether the dependencies exist (in developing flow) or independence is observed (in fully developed flow) [32,33]. Hao Ma et al. [34] investigated laminar nanofluid flow and heat transfer through micro-tubes in the entry region. The study considered microtubes with constant wall temperature and constant heat flux boundary conditions using a multiphase Euler-Lagrangian method. The effects of various factors such as Peclet number (between 175 and 3500), nanoparticle volume density (between 0.1% and 1.0%) and nanoparticle diameter (between 40 and 130 nm) on the thermal characteristics of Al_2O_3-water nanofluid flow were analysed. Their findings indicated that both the Reynolds number's impact on the friction factor and the influence of axial heat conduction on the Nusselt number need to be considered in the entry region.

The hydrodynamic entry length X_{hy} represents the length necessary for the centerline velocity to reach 99% of its fully developed value [35]. Several experimental and theoretical results $X_{hy} = f(\mathrm{Re})\, D_{in}$, as a function of Reynolds number for the base fluid flow and the inner diameter D_{in} of a horizontal pipe, have been published in [36]. Atkinson et al. [37] employed numerical methods to derive an expression for the laminar hydrodynamic entry length in horizontal circular pipes as

$$X_{hy} = (0.59 + 0.056\ \mathrm{Re})\, D_{in}\,, \qquad 1 < \mathrm{Re} < 1000. \tag{1.1}$$

Durst et al. [38] investigated the development length of laminar pipe flow applying the finite volume method as

$$X_{hy} = [0.619^{1.6} + (0.0567\mathrm{Re})^{1.6}]^{\frac{1}{1.6}}\, D_{in}\,, \qquad 0.1 < \mathrm{Re} < 2300. \tag{1.2}$$

Joshi et al. [39] conducted numerical simulations of laminar pipe flows of a Newtonian flow with no-slip condition to understand the effect of inlet conditions on entry lengths, they suggested the correlation as

$$X_{hy} = \big(-0.0437 + 0.0553\ \mathrm{Re} + 0.413\ exp(-0.1\ \mathrm{Re})\big) D_{in}\,, \quad 0.001 < \mathrm{Re} < 2300. \tag{1.3}$$

Heat applied to a pipe's surface causes neighboring fluid particles to equilibrate, resulting in a temperature difference between the surface and the pipe's central axis. This variation induces radial convectional heat transfer, forming a thermal boundary layer that expands along the pipe's length until it merges at the center. The thermal inlet length in laminar flow is the distance along which heating is required to bring the Nusselt number to close to 105% of the theoretical fully developed value of 4.36 under constant heat flux boundary condition [40].

Nguyen [41] investigated laminar pipe flow with a constant heat flux boundary condition using finite difference method to introduce the following relationship for the thermal entry length

$$X_{th} = \left(0.5163 + \frac{0.1463}{\mathrm{Re}}\right) D_{in}, \qquad 20 < \mathrm{Re} < 1000. \tag{1.4}$$

1.1. MONO AND HYBRID NANOFLUIDS

Nanofluids, with their unique ability to enhance heat transfer characteristics, have been classified into two primary types: mono and hybrid nanofluids. Each type offers distinct advantages and considerations, influencing their selection based on specific application requirements and desired thermal attributes.

MONO NANOFLUIDS

Mono nanofluids are comprised of a single type of nanoparticle uniformly dispersed within a base fluid, such as water or oil. These nanofluids exhibit enhanced thermophysical properties compared to their base fluids due to the presence of nanoparticles, which can include materials like metal oxides, carbon nanotubes, or metallic nanoparticles. The addition of nanoparticles alters the thermal conductivity, viscosity, and other properties of the base fluid, making mono nanofluids promising candidates for various applications such as heat transfer enhancement in thermal systems, lubrication, and cooling in electronics. Their homogeneous nature simplifies manufacturing processes and ensures consistent performance, offering potential benefits in diverse industrial and scientific fields.

HYBRID NANOFLUIDS

In contrast, hybrid nanofluids incorporate a mix of different nanoparticle types within the base fluid, creating a synergistic effect. This complex composition offers a combination of the individual benefits of each nanoparticle type, providing an enhanced and tailored thermal performance. The synergy achieved in hybrid nanofluids results in unique thermal properties not attainable with mono nanofluids. By combining nanoparticles with diverse thermal conductivities, shapes, and sizes, hybrid nanofluids can exhibit improved heat transfer efficiency over a broader range of conditions. Hybrid nanofluids find applications in situations where a more versatile and adaptive heat transfer solution is needed. For instance, in solar thermal systems, where the heat transfer fluid must operate under varying temperature and radiation conditions, hybrid nanofluids can offer superior performance due to their diverse nanoparticle composition.

SELECTION CRITERIA

The choice between mono and hybrid nanofluids is not arbitrary; it depends on the specific demands of the intended application. Several factors influence this decision:

1. **Application Requirements:**
    - Mono nanofluids are favored when a straightforward enhancement in heat transfer is sufficient for the application.
    - Hybrid nanofluids are chosen when a more adaptive thermal performance is needed, especially in applications with variable operating conditions.

2. **Desired Thermal Attributes:**
    - If a consistent and easily controllable thermal behavior is required, mono nanofluids may be the preferred choice.
    - For applications demanding enhanced heat transfer over a wider range of conditions, hybrid nanofluids offer a more versatile solution.

3. **Manufacturing Considerations:**

   - The simplicity of formulation favors mono nanofluids in scenarios where ease of production and stability are critical.
   - Hybrid nanofluids, with their more complex composition, may require additional manufacturing considerations but can provide superior performance tailored to specific needs.

In conclusion, the choice between mono and hybrid nanofluids involves a careful consideration of application requirements and desired thermal attributes. While mono nanofluids offer simplicity and predictability, hybrid nanofluids provide a more sophisticated solution with the potential for superior performance in diverse operating conditions. As research in nanofluid technology advances, a deeper understanding of these variations will undoubtedly lead to more targeted and effective applications, pushing the boundaries of heat transfer efficiency across industries.

1.2. TYPES OF NANOPARTICLES

Nanoparticles introduce a realm of possibilities with their diverse characteristics. Beyond the material composition, the size, shape, and diameter of nanoparticles, coupled with the volume fraction, wield a profound influence on nanofluid performance in the realm of heat transfer. This comprehensive exploration delves into the intricate interplay between these factors, shedding light on the fascinating dimensions that shape nanofluid behavior.

METALLIC NANOPARTICLES: COPPER, ALUMINUM

Metallic nanoparticles, such as copper and aluminum, are revered for their exceptional thermal conductivity. These materials, when introduced into nanofluids, bring about a remarkable enhancement in heat transfer capabilities. The efficient conduction of heat through metallic nanoparticles makes them pivotal in applications where thermal management is paramount.

OXIDE-BASED STABILITY: ALUMINA AND SILICA

Oxide-based nanoparticles, like alumina and silica, offer stability and versatility. Beyond their stability in suspension, these nanoparticles exhibit versatile properties that extend their applications from electronics cooling to advanced manufacturing processes. Their unique characteristics contribute to the overall thermal behavior of nanofluids.

CARBONACEOUS NANOPARTICLES: GRAPHENE AND CARBON NANOTUBES

Carbon-based nanoparticles, represented by graphene and carbon nanotubes, bring a blend of lightweight strength and high thermal conductivity. These materials, known for their exceptional mechanical properties, find applications in nanofluids where both robustness and heat transfer efficiency are critical.

Spherical Symmetry: Maximum Dispersion

Spherical nanoparticles, characterized by their symmetrical shape, frequently attract attention in the creation of nanofluid compositions. Their well-defined shape facilitates improved dispersion within the base fluid, preventing agglomeration and ensuring a homogeneous mixture. Beyond dispersion, spherical nanoparticles exhibit enhanced thermal conductivity, making them a popular choice for applications demanding predictable and consistent heat transfer performance.

Non-Spherical Nanoparticles: Rods, Platelets, and Thermal Uniqueness

While spherical nanoparticles dominate certain applications, non-spherical counterparts introduce a variety of thermal characteristics. Rod-like or platelet-shaped nanoparticles, for instance, may influence fluid flow patterns and heat transfer mechanisms in distinctive ways. This non-uniformity in shape gives rise to unique thermal behaviors, allowing for tailored solutions in specific applications.

The Diameter: Small versus Large

Nanoparticle diameter emerges as a critical factor in the heat transfer equation. Smaller nanoparticles, with their increased surface area per unit volume, maximize interactions with the base fluid, promoting efficient convective heat transfer. Conversely, larger nanoparticles may present challenges related to dispersion and fluid flow, requiring a delicate balance between diameter and thermal advantages.

1.3. TYPES OF BASE FLUIDS

In the dynamic realm of nanofluid formulation, the choice of a base fluid stands as a critical decision, exerting a profound influence on the overall performance of the nanocomposite fluid. While water-based nanofluids have dominated research due to their exceptional thermal properties, the landscape expands further into oil-based nanofluids and beyond. This exploration delves into the considerations, advantages, and challenges associated with different base fluids, underscoring the importance of using nanofluids to the specific thermal, chemical, and environmental demands of diverse applications.

Water-Based Nanofluids

Water, with its high thermal conductivity and specific heat capacity, has become the quintessential base fluid for nanofluids. The outstanding thermal properties of water make it an ideal candidate for applications where efficient heat transfer is paramount.

- **Applications**

Water-based nanofluids find widespread use in various industries, ranging from electronics cooling to solar thermal systems. Their ability to efficiently dissipate heat makes them indispensable in scenarios where maintaining optimal temperatures is crucial for performance and longevity.

- **Challenges**

Despite their exceptional properties, water-based nanofluids pose challenges related to stability and potential particle agglomeration. Researchers continually explore strategies to enhance stability and mitigate these challenges for practical applications.

Oil-Based Nanofluids

In scenarios where water is unsuitable due to its electrical conductivity or chemical interactions, oil-based nanofluids present a viable alternative. The dielectric properties of oil make it suitable for applications where electrical insulation is a priority.

- **Enhanced Stability**

Oil-based nanofluids often exhibit improved stability compared to their water-based counterparts. This stability can be advantageous in applications where prolonged shelf life and consistent performance are essential.

- **Limitations**

However, oil-based nanofluids may face challenges related to lower thermal conductivity compared to water-based counterparts. The choice between water and oil as a base fluid depends on the specific trade-offs acceptable for the intended application.

Using Nanofluids to Application Requirements

The choice of a base fluid is intricately tied to the specific thermal, chemical, and environmental demands of the intended application. Using nanofluids to meet these requirements involves a good understanding of the advantages and limitations of each base fluid option.

Considerations in Base Fluid Selection:

1. **Thermal Conductivity Requirements:** Assessing the required thermal conductivity for efficient heat transfer.
2. **Chemical Compatibility:** Ensuring compatibility between the base fluid and nanoparticles to prevent undesirable reactions.

3. **Environmental Impact:** Evaluating the environmental impact of the base fluid, especially in applications where sustainability is a concern.

Innovations in Base Fluid Selection

As nanofluid research progresses, the quest for optimal base fluids continues. Emerging technologies, such as the integration of smart fluids and bio-based fluids, promise to revolutionize the landscape of nanofluids, offering tailored solutions for diverse applications.

In conclusion, the selection of a base fluid for nanofluids is a multifaceted decision that requires a careful balance of thermal properties, stability, and compatibility. Water and oil, as traditional choices, have paved the way for diverse applications. Still, the exploration of novel base fluids opens doors to innovations that can redefine the capabilities of nanofluids in addressing complex heat transfer challenges across various industries. As researchers continue to unravel the complexities and possibilities, the future holds exciting prospects for the evolution of base fluids in nanofluid technology.

1.4. APPLICATIONS OF NANOFLUIDS

Nanofluids, colloidal suspensions of nanoparticles in a base fluid, have emerged as a transformative technology with the potential to revolutionize heat transfer across various industries. The integration of nanoparticles into conventional fluids imparts unique thermal properties, paving the way for enhanced heat transfer performance. This exploration delves into the diverse applications of nanofluids, showcasing their ability to address complex thermal challenges and optimize heat exchange processes.

Electronics Cooling: Maintaining Optimal Temperatures

In the realm of electronics, managing heat dissipation is crucial for maintaining the performance and reliability of electronic components. Nanofluids offer a cutting-edge solution by efficiently conducting and dissipating heat. Water-based nanofluids, often containing metallic nanoparticles like copper, prove to be particularly effective in cooling electronic devices. Their high thermal conductivity and stability aid in preventing overheating, contributing to the longevity and efficiency of electronic systems.

Automotive Engines: Enhancing Thermal Management

The automotive industry has embraced nanofluids as a means to optimize thermal management in engines. Nanofluids, with their improved heat transfer capabilities, enable more efficient cooling of engine components. This enhanced thermal management contributes to increased fuel efficiency, reduced emissions, and improved overall engine performance. The versatility of nanofluids allows using formulations to meet the specific demands of different engine types and operating conditions.

Solar Thermal Systems: Boosting Energy Harvesting

Nanofluids play a pivotal role in solar thermal systems, where efficient heat transfer is essential for maximizing energy harvesting. Nanofluids, often utilizing oxide-based nanoparticles, exhibit enhanced thermal conductivity and can operate at elevated temperatures. This makes them well-suited for applications like solar collectors, where they facilitate the absorption and transfer of solar energy, contributing to improved overall system efficiency.

Biomedical Applications: Precision in Thermal Therapy

In the field of medicine, nanofluids are harnessed for precise thermal control in biomedical applications. Magnetic nanoparticles, such as iron oxide, are introduced into nanofluids for applications like hyperthermia—a therapeutic technique that involves heating targeted tissues. The precise control over temperature afforded by nanofluids ensures effective treatment while minimizing damage to surrounding healthy tissues.

HVAC Systems: Optimizing Heating, Ventilation, and Air Conditioning

Nanofluids have found their way into Heating, Ventilation, and Air Conditioning (HVAC) systems, where efficient heat transfer is fundamental. By incorporating nanofluids, HVAC systems can achieve improved thermal performance, resulting in enhanced energy efficiency and reduced operating costs. The ability to customize nanofluid formulations based on the specific requirements of HVAC systems demonstrates the versatility and adaptability of nanofluid technology.

Advanced Manufacturing Processes: Precision Cooling and Heating

In manufacturing processes, nanofluids contribute to precision cooling and heating, ensuring optimal conditions for various industrial applications. Whether in metalworking, plastics processing, or other manufacturing operations, nanofluids facilitate controlled and efficient heat transfer. The ability to tailor nanofluid properties to match the specific thermal demands of diverse manufacturing processes underscores their potential in advancing industrial technologies.

Challenges

While hybrid nanofluids are generally known to exhibit improved heat transfer capabilities, there are still some challenges. First of all, there is a lack of agreement among the theoretical models in predicting the specific behaviour of hybrid nanofluids. Moreover, there is a misinterpretation among the scholars. Finally, various approaches provide various results for the same hybrid nanofluid and nanoparticle volume fraction during the preparation step [18]. While the application of nanofluids for enhancing heat transfer performance is promising, challenges remain. Issues related to stability, cost, and potential environmental impacts necessitate ongoing research and development. Addressing these challenges will be crucial in realizing the full potential of nanofluids across industries. Looking ahead, the future of nanofluids in heat transfer applications holds exciting possibilities. Continued research into novel nanoparticle formulations, improved manufacturing processes, and a deeper understanding of the underlying mechanisms will unlock new frontiers. As nanofluid technology evolves, its integration into various sectors promises to redefine standards in heat transfer efficiency, opening doors to innovative solutions for the challenges of tomorrow.

1.5. THE AIM OF THIS THESIS

The aim of this thesis is to investigate and analyse the heat transfer enhancement characteristics of various nanofluids in laminar flow configurations within horizontal pipes. This research endeavours to contribute to the understanding of convective heat transfer phenomena in nanofluid systems.

The first objective is to examine the influence of different nanoparticle types and concentrations on heat transfer enhancement. Through numerical simulations, the study evaluates nanofluids comprised of Al_2O_3, CuO, MWCNT, TiO_2, and Ag nanoparticles dispersed in base fluids such as engine oil and water. The analysis encompasses a range of volume fractions, investigating their impact on convective heat transfer coefficients and Nusselt numbers under steady-state conditions.

Additionally, this research aims to explore the relationship between flow rates, nanoparticle concentrations, and thermal boundary conditions on heat transfer performance. By employing computational fluid dynamics techniques, the study investigates the hydrodynamic behaviour of nanofluids, velocity distributions, wall shear stress, and skin friction coefficients. Furthermore, the investigation extends to obtain the thermal boundary layer profiles along the pipe length, providing insights into the intricate interactions between fluid flow and heat transfer.

Another crucial aspect of this thesis is the assessment of temperature-dependent thermophysical properties in nanofluid simulations. By comparing the accuracy of simulation results obtained using both constant and temperature-dependent properties, this research endeavours to enhance the predictive capability of numerical models in capturing the complex thermohydraulic behaviour of nanofluids.

Furthermore, this thesis aims to establish correlations for the hydrodynamic entry length and thermal entry length, offering valuable insights into the flow characteristics of nanofluids. Through comprehensive analyses, including the examination of Performance Efficiency Index (PEI), this research seeks to optimize the design and operation of systems utilizing nanofluids for enhanced heat transfer performance.

Overall, this thesis aspires to contribute to the advancement of knowledge in the field of nanofluid heat transfer, providing valuable insights into the optimization of nanofluid-based systems for various engineering applications.

1.6. FUTURE PLAN

Future studies may explore the effects of other parameters, such as the shape of nanostructures, to assess their impact on heat transfer performance [42]. Furthermore, future research should examine different mixture ratios of nanoparticles in hybrid nanofluids. It is essential to emphasize that a considerable number of numerical studies do not take into account the non-Newtonian behaviour exhibited by nanofluids. Consequently, there is a need for additional research to explore the non-Newtonian properties associated with the flow of nanofluids [43]. Moreover, expanding the scope of investigation to include turbulent flow regimes within horizontal pipes could provide a comprehensive understanding of nanofluid behaviour across a wider range of operating conditions. Additionally, experimental validation of the numerical simulations would strengthen the reliability and applicability of the findings. Exploring the effects of additional parameters such as surface roughness, pipe diameter, and aspect ratio on heat transfer enhancement could offer deeper insights into the optimization of nanofluid systems. Moreover, investigating novel nanoparticle combinations and base fluids could unveil potential advancements in heat transfer performance. Integration of advanced machine learning techniques for data analysis and prediction could enhance the predictive capabilities of the models, facilitating the design of more efficient nanofluid-based heat transfer systems. Overall, future research endeavours should aim to address these aspects to further advance the field and foster practical applications in various engineering domains.

2. THERMOPHYSICAL PROPERTIES

The heat transfer efficiency in a nanofluid is significantly influenced by factors such as its viscosity, thermal conductivity, density, and specific heat [44]. In the following discussion, the thermophysical properties of different nanofluids will be presented, like Al_2O_3-water, Al_2O_3-engine oil, CuO-engine oil, CuO:MWCNT-oil, CuO-water, TiO_2-water, and Ag-water. Each nanofluid has unique characteristics such as thermal conductivity and viscosity, essential for various engineering applications.

2.1. AL$_2$O$_3$-WATER NANOFLUID

To compare and analyze the influence of temperature-dependence on the numerical results, the thermophysical properties of Al_2O_3-water nanofluids are considered to be constant or temperature-dependent.

2.1.1. CONSTANT THERMOPHYSICAL PROPERTIES

Properties of alumina Al_2O_3 at 298.15K are presented in Table 2.1 [45].

Table 2.1 Density, heat capacity, and thermal conductivity of alumina and water.

Property	Al_2O_3	water
ρ (kg/m^3)	3650	998.3
C_P (J/kgK)	765	4182
k (W/mK)	40	0.6

The thermophysical properties of the nanofluid flow are calculated at the average bulk temperature, i.e. $T_{nf_{(avg)}} = (T_{nf_{(out)}} + T_{nf_{(in)}})/2$.

To predict the density and heat capacity of the nanofluid, the following correlations are employed [46]

$$\rho_{nf} = \varphi\rho_{np} + (1-\varphi)\rho_{bf}, \tag{2.1}$$

$$C_{p_{nf}} = \frac{\varphi\rho_{np}C_{p_{np}} + (1-\varphi)\rho_{bf}C_{p_{bf}}}{\rho_{nf}}, \tag{2.2}$$

where φ denotes the nanoparticle volume fraction. The dynamic viscosity of the nanofluid is predicted using the Klazly-Bognar viscosity model [47]

$$\mu_{nf} = \mu_{bf}(1 + 9.4974\varphi + 77.811\varphi^2 + 0.9514\varphi^3). \tag{2.3}$$

The thermal conductivity of the nanofluid is calculated using the modified Maxwell equation as given [48]

$$k_{nf} = k_{bf}\left[\frac{k_{np}+2k_{bf}+2(k_{np}-k_{bf})(1+\beta)^3\varphi}{k_{np}+2k_{bf}-(k_{np}-k_{bf})(1+\beta)^3\varphi}\right], \tag{2.4}$$

with $\beta = 0.1$.

2.1.2. TEMPERATURE-DEPENDENT THERMOPHYSICAL PROPERTIES

The thermophysical properties of water, as the base fluid, are considered as a function of temperature presented in [49], when T is given in Kelvin:

$$\rho_{bf}(T) = 10^3 - \frac{(T-277.1363)^2(T+15.7914)}{5.089292\ 10^2(T-205.0204)}, \tag{2.5}$$

$$C_{p_{bf}}(T) = -1.41414\ \ 10^{-4}\,T^3 + 0.1444662\,T^2 - 48.73648329\,T + 9616.873445, \tag{2.6}$$

$$k_{bf}(T) = -1.315\ \ 10^{-5}\,T^2 + 9.734\ \ 10^{-3}\,T - 1.1245, \tag{2.7}$$

$$\mu_{bf}(T) = 1.7184\,10^{-7}\,T^2 - 1.208\ \ 10^{-4}\,T + 2.165\ \ 10^{-2}. \tag{2.8}$$

These relationships are used in relationships (2.1)-(2.4) to calculate the density, heat capacity, thermal conductivity, and dynamic viscosity of the nanofluid in case of temperature-depend thermophysical properties. Note that these relationships are valid in the temperature range 274-352*K*, which covers the temperature range used in my simulations.

2.2. CUO-WATER NANOFLUID (constant properties)

The density and heat capacity of the nanofluid are calculated using equations (2.1)-(2.2). The viscosity of nanofluid μ_{nf} is obtained from below equation, which is called Brinkman equation as follows [50,51]

$$\mu_{nf} = \frac{\mu_{bf}}{(1-\varphi)^{2.5}}, \tag{2.9}$$

where μ_{bf} is the viscosity of the base fluid (water), and φ refers to nanoparticle volume fraction.

The thermal conductivity of nanofluid k_{nf} is given as follows [52]

$$k_{nf} = k_{bf}\frac{k_{np}+2k_{bf}-2\varphi(k_{bf}-k_{np})}{k_{np}+2k_{bf}+\varphi(k_{bf}-k_{np})}, \tag{2.10}$$

where k_{bf} is the thermal conductivity of base fluid, and k_{np} is the thermal conductivity of the nanoparticles.

Thermophysical properties for pure water and nanoparticles are given in Table 2.2.

Table 2.2. Thermophysical properties for pure water and CuO nanoparticles [53].

Property	CuO	Pure water
ρ *(kg/m^3)*	6500	998.2
C_P *(J/kgK)*	535.6	4182
k *(W/mK)*	20	0.6
μ *(Ns/m^2)*	-	0.001003

Thermophysical properties for CuO-water nanofluid at different values of φ are presented in Table 2.3.

Table 2.3. Thermophysical properties for CuO-water at different values of φ.

Property	CuO-water			
	φ =1%	φ =2%	φ =3%	φ =4%
ρ_{nf} *(kg/m^3)*	1053.218	1108.236	1163.254	1218.272
C_{pnf} *(J/kg K)*	3956.96	3754.26	3570.74	3403.79
k_{nf} *(W/m K)*	0.6166	0.6335	0.6508	0.6683
μ_{nf} *(Ns/m^2)*	0.00102852	0.001054959	0.00108236	0.001110767

2.3. TIO$_2$-WATER NANOFLUID AND AG-WATER NANOFLUID (CONSTANT PROPERTIES)

Density, heat capacity, and thermal conductivity of TiO$_2$ and Ag nanoparticles at 298.15K are presented in Table 2.4.

Table 2.4. Density, heat capacity, and thermal conductivity of the nanoparticles [54,55].

Property	TiO$_2$	Ag
ρ *(kg/m^3)*	4170	10500
C_P *(J/kgK)*	711	235
k *(W/mK)*	11.8	429

Thermophysical properties of TiO$_2$-water Nanofluid and Ag-water Nanofluid are taken temperature-dependent as [46,49]

$$\rho_{nf}(T) = \varphi\rho_{np} + (1-\varphi)\rho_{bf}(T)\,, \tag{2.11}$$

$$C_{p_{nf}}(T) = \frac{\varphi\rho_{np}C_{p_{np}} + (1-\varphi)\rho_{bf}(T)C_{p_{bf}}(T)}{\rho_{nf}(T)}\,, \tag{2.12}$$

where φ is the nanoparticle volume fraction, which can vary between 0 and 1. T is given in Kelvin. The viscosity of the nanofluids is calculated by Klazly-Bognar viscosity model as [47]

$$\mu_{nf}(T) = \mu_{bf}(T)(1 + 9.4974\varphi + 77.811\varphi^2 + 0.9514\varphi^3). \tag{2.13}$$

The thermal conductivity of the nanofluids are calculated as [48]

$$k_{nf}(T) = k_{bf}(T)\left[\frac{k_{np}+2k_{bf}(T)+2(k_{np}-k_{bf}(T))(1+\beta)^3\varphi}{k_{np}+2k_{bf}(T)-(k_{np}-k_{bf}(T))(1+\beta)^3\varphi}\right], \tag{2.14}$$

where $\beta = 0.1$ is a constant to consider the effect of nanolayer thickness on the thermal conductivity of the nanofluid. Thermophysical properties of the base fluid (water) as a function of temperature are calculated by relationships (2.5)-(2.8).

2.4. CUO:MWCNT-OIL NANOFLUID (constant properties)

In Table 2.5, the characteristics of the engine oil as a base fluid at a temperature of 45 degrees Celsius, Copper Oxide (CuO), and Multi-Walled Carbon Nanotubes (MWCNT) are displayed.

Table 2.5. Thermophysical properties of the engine oil (base fluid) at T=45 ℃, CuO, and MWCNT.

Property	CuO [56]	MWCNT [56]	Engine Oil [57]
ρ (kg/m^3)	6400	2100	848.5
C_P (J/kgK)	531.02	735	1975
k (W/mK)	76.5	3000	0.1215
μ (Ns/m^2)	-	-	0.02442832

2.4.1. DENSITY: MONO AND HYBRID NANOFLUID

The equation provided by Pak and Cho [58] was utilized to accurately estimate the density of mono nanofluids as given by

$$\rho_{mnf} = \varphi_{np}\rho_{np} + (1-\varphi_{np})\rho_{bf}\ , \tag{2.15}$$

where φ_{np} denotes volume fraction of nanoparticle for mono nanofluid. Takabi [59] modified the rule of mixing and provided the following equation for hybrid nanofluids as follows

$$\rho_{hnf} = \varphi_{np,1}\rho_{np,1} + \varphi_{np,2}\rho_{np,2} + (1-\varphi_{hnp})\rho_{bf}\ , \tag{2.16}$$

where $\varphi_{np,1}$ and $\varphi_{np,2}$ denote the nanoparticle volume fractions of the first and the second nanopartilce, respectively. φ_{hnp} represents the total nanoparticle volume fraction which is $\varphi_{hnp} = \varphi_{np,1} + \varphi_{np,2}$. Using correlations (2.15) and (2.16), the changes in density with nanoparticle volume fraction for CuO-oil, MWCNT-oil, and CuO:MWCNT-oil nanofluids are depicted in Fig. 2.1. The density for all nanofluids shows an increasing trend with increasing the nanoparticle volume fraction. It should be noted that the increase in density for CuO-oil nanofluid is greater compared to that observed in other nanofluids.

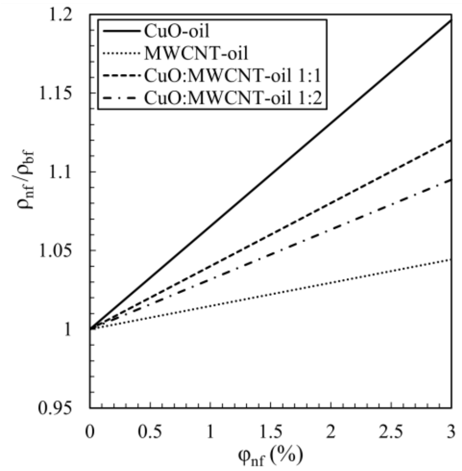

Fig. 2.1. The relative density variation with volume fraction for different nanofluids at T=45 ˚C.

2.4.2. SPECIFIC HEAT CAPACITY: MONO AND HYBRID NANOFLUID

The first calculation of the specific heat capacity for a mono nanofluid was conducted by Pak et al. [58], who applied the mixture rule while assuming thermal balance between the nanoparticles and the base fluid. The formula is given as

$$C_{P_{mnf}} = \frac{\varphi_{np}\rho_{np}C_{P_{np}}+(1-\varphi_{np})\rho_{bf}C_{P_{bf}}}{\rho_{mnf}}. \quad (2.17)$$

Takabi et al. [59] presented the specific heat capacity for a hybrid nanofluid as

$$C_{P_{hnf}} = \frac{\varphi_{np,1}\rho_{np,1}C_{P_{np,1}}+\varphi_{np,2}\rho_{np,2}C_{P_{np,2}}+(1-\varphi_{hnp})\rho_{bf}C_{P_{bf}}}{\rho_{hnf}}. \quad (2.18)$$

Applying correlations (2.17) and (2.18), the heat capacity for CuO-oil, MWCNT-oil, and CuO:MWCNT-oil nanofluids is depicted in Fig. 2.2. The heat capacity of nanofluids shows a decreasing behavior with increasing the nanoparticle volume fraction. The reduction in density for CuO-oil nanofluid is greater than that observed in the other three nanofluids.

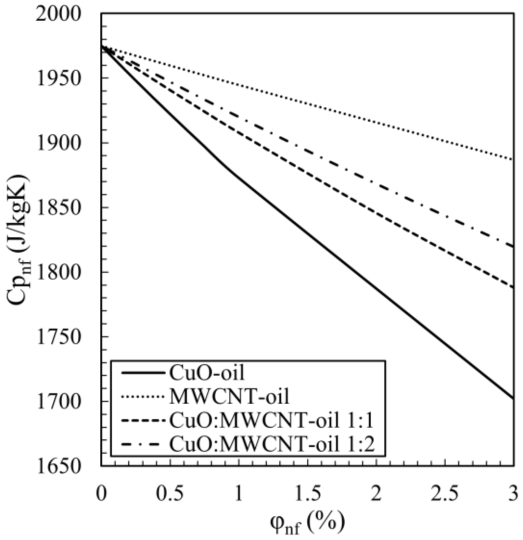

Fig. 2.2. The relative heat capacity variation with volume fraction for different nanofluids at $T = 45^{\circ}C$.

2.4.3. THERMAL CONDUCTIVITY: MONO AND HYBRID NANOFLUID

The modified Hamilton and Crosser model [60] is employed to determine the thermal conductivity of mono nanofluid as expressed

$$k_{mnf} = k_{bf}\left(\frac{k_{np}+2k_{bf}-2\varphi_{np}\left(k_{bf}-k_{np}\right)}{k_{np}+2k_{bf}+\varphi_{np}\left(k_{bf}-k_{np}\right)}\right). \tag{2.19}$$

For hybrid nanofluid the modified Hamilton and Crosser model [59] is applied as given

$$k_{hnf} = k_{bf}\left(\frac{\frac{\varphi_{np,1}k_{np,1}+\varphi_{np,2}k_{np,2}}{\varphi_{hnp}}+2k_{bf}+2\left(\varphi_{np,1}k_{np,1}+\varphi_{np,2}k_{np,2}\right)-2\varphi_{hnp}k_{bf}}{\frac{\varphi_{np,1}k_{np,1}+\varphi_{np,2}k_{np,2}}{\varphi_{hnp}}+2k_{bf}-\left(\varphi_{np,1}k_{np,1}+\varphi_{np,2}k_{np,2}\right)+\varphi_{hnp}k_{bf}}\right). \tag{2.20}$$

Using equations (2.19) and (2.20), the thermal conductivity for CuO-oil, MWCNT-oil, and CuO:MWCNT-oil nanofluids is depicted in Fig. 2.3. It is noteworthy that the thermal conductivity augmentation in MWCNT-oil nanofluid exceeds that observed in the other nanofluids.

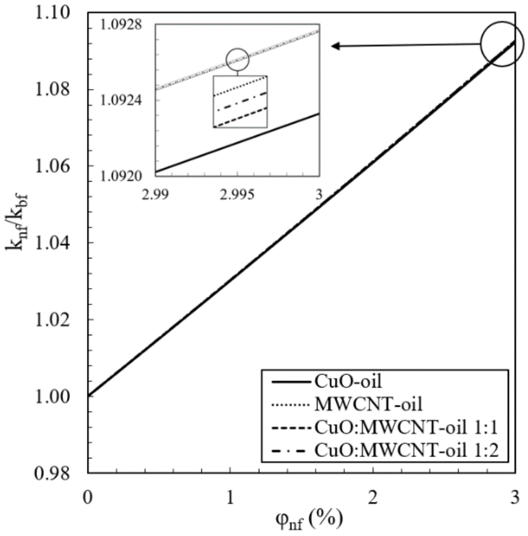

Fig. 2.3. The relative thermal conductivity variation with volume fractions for different nanofluids at $T = 45^\circ C$.

2.4.4. DYNAMIC VISCOSITY: MONO AND HYBRID NANOFLUID

The addition of nanoparticles to a fluid results in an increase in its viscosity [44]. Indeed, introducing nanofluids to based fluids, even at very low concentrations, increases the nanofluid's viscosity. The key explanation for this rise is that when the volume fraction grows, the chance of the nanofluids' cluster developing increases. The presence of nanoclusters impedes the movement of fluid layers, and consequently intensifies the nanofluid's viscosity. The Batchelor model is employed to calculate the viscosity of mono nanofluid [61] as follows

$$\mu_{mnf} = \mu_{bf}\left(1 + 2.5\varphi_{np} + 6.2{\varphi_{np}}^2\right) . \tag{2.21}$$

Accordingly, to determine the dynamic viscosity of hybrid nanofluid, the Batchelor model [59] can also be used as

$$\mu_{hnf} = \mu_{bf}\left(1 + 2.5\varphi_{hnp} + 6.2{\varphi_{hnp}}^2\right) . \tag{2.22}$$

Note that these two correlations for dynamic viscosity depend only on the nanoparticle volume fraction. Therefore, different nanofluids with the same nanoparticle volume fraction reveal the same amount of dynamic viscosity.

3. GEOMETRY, MESH GENERATION, AND CFD PROCEDURE

In simulating nanofluid flow within a pipe using Computational Fluid Dynamics (CFD), the process involves several key steps. First, the geometry of the pipe system is defined, detailing its dimensions and layout. Then, a computational mesh is generated to discretize the domain, with a focus on refining near walls to capture boundary layer effects accurately. The CFD procedure includes setting up the problem by defining boundary conditions and selecting appropriate mathematical models and numerical methods. The solver is configured accordingly, and the simulation is run to solve the governing equations iteratively. Post-processing techniques are then applied to analyse and visualize the results, providing insights into velocity profiles and temperature distributions within the pipe. Through this process, CFD facilitates the study of nanofluid behaviour in pipes, aiding various engineering applications.

3.1. GEOMETRY AND MESH GENERATION

In case of Al_2O_3-water nanofluid: The nanofluid flows through a circular horizontal pipe of a length L=1m and diameter D_{in}=7 mm (see Fig. 3.1) with uniform inlet temperature and velocity distributions are experimentally investigated by Esmaeilzadeh et al. [62]. The same geometry is created using Design Modeler and a three-dimensional flow case is chosen to match the experimental set-up. Adjacent to the pipe wall, the applied cells are thinner. The cells close to the walls are also adequately dense because the temperature gradients are higher than those in other areas. Figure 3.2 shows the creation of a boundary layer mesh for optimizing the fluid flow features by thin components adjacent to the pipe wall.

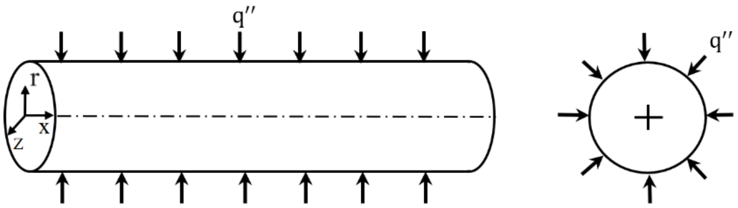

Fig. 3.1. Three-dimensional geometry of the circular horizontal pipe.

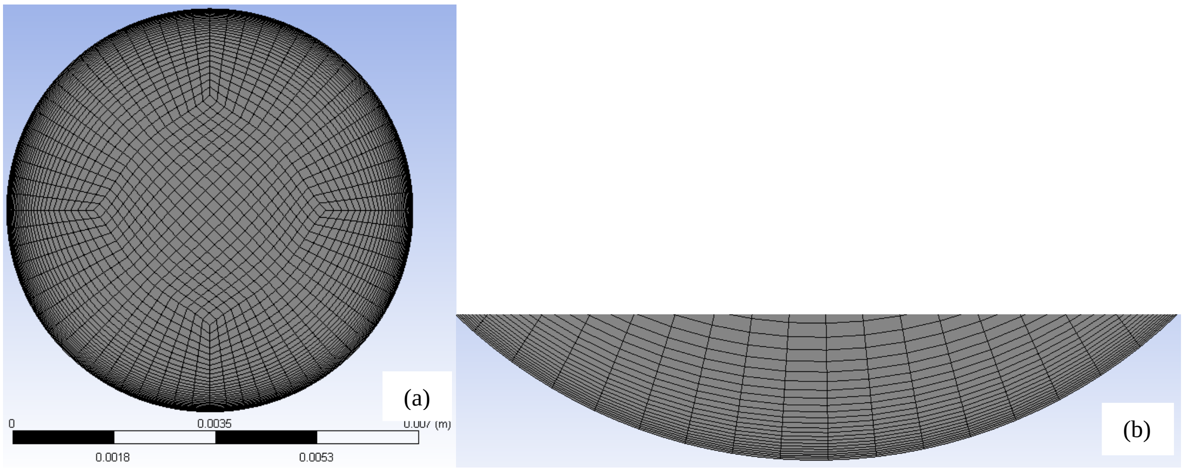

Fig. 3.2. (a) Mesh geometry across the pipe cross section (b) Mesh boundary layer adjacent to the wall.

To analyse mesh grid independence, the average values for the Nusselt number and friction factor, for the pure water at Re=799.53 for a wide range of mesh sizes are investigated. Based on a comprehensive examination of the solution independence of a mesh, it is observed that the mesh with 830,415 elements can produce the most accurate results (see Fig. 3.3) and it is used in the simulations.

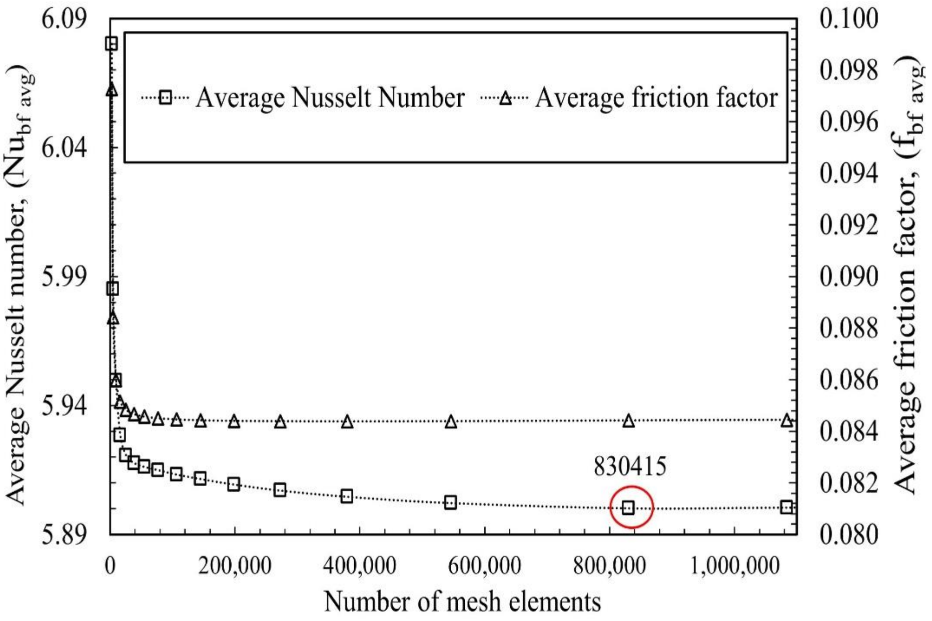

Fig. 3.3. Mesh independence test (average Nusselt number and the average friction factor).

In case of CuO-water nanofluid: Figure 3.4 demonstrates the geometry and the computational domain schematically. The channel's diameter and length have been set at 0.1m and 2m, respectively. With a temperature of 275*K* and a velocity given by Reynolds numbers equal to 1000 (Re=1000), the flow at the inlet has been assumed to be hydrodynamically steady. The lower wall receives a constant heat flux of 200 W/m^2 from downside, while the upper wall is set to be adiabatic from up. The geometry is created by using DesignModeler of official Ansys Fluent, and the two-dimensional flow problem in single-phase was selected.

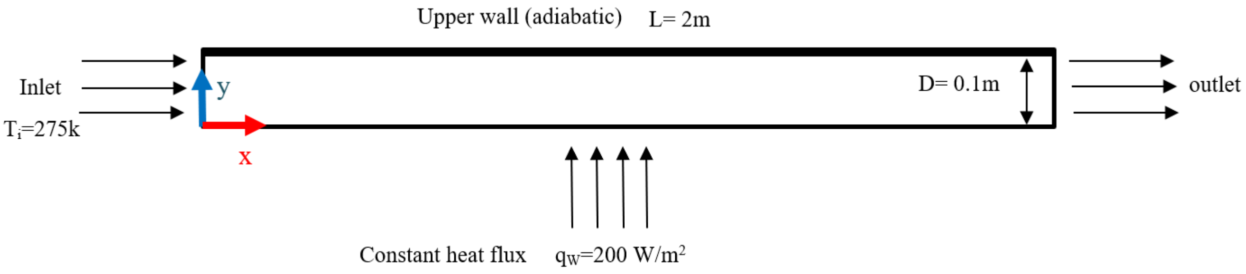

Fig. 3.4. The schematic diagram of the computational domain.

Mesh Generation: Non-uniform quadrilateral grid system is employed for meshing the domain generated by Meshing of official Ansys Fluent as shown in Fig. 3.5.

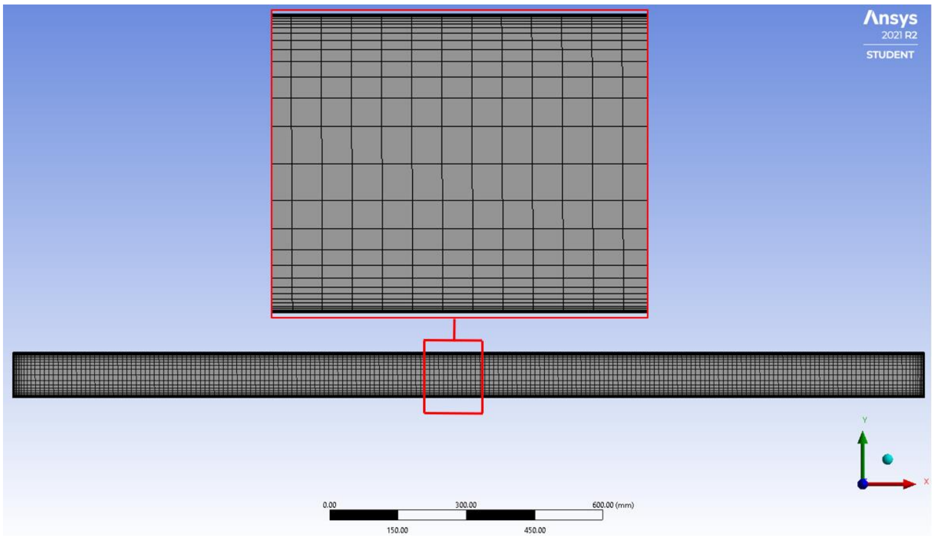

Fig. 3.5. Mesh generation for the model.

Because the accuracy of finite volume technique is strongly related to the quality of the discretization utilized, the grid independence test is performed to confirm that the given solution is mesh independent. As a result, a precise mesh sensitivity investigation was conducted in order to reduce the numerical impacts imposed by mesh size. The mesh sensitivity was examined for four meshes, and the test compared the average Nusselt number on the bottom wall for each mesh. The results are shown in Table 3.1. The Nusselt number for mesh 3 with 12400 cells was determined to be adequate for ensuring the accuracy of the solution as well as the grid's independence.

Table 3.1. Mesh independency investigation.

Mesh	Number of cells	Average Nusselt number
1	2400	23.88086
2	6390	24.15811
3	**12400**	**24.25852**
4	20250	24.30758

In case of CuO: MWCNT-oil nanofluid: The nanofluid flows inside a three-dimensional pipe with the length of $L=1.3m$, and inner diameter of $D_{in}=7\ mm$ (see Fig. 3.1) as it was investigated in the experimental study conducted by Heris et al. [57]. Utilizing Design Modeler, the geometry is created, and the three-dimensional flow case is selected in accordance with the experimental set-up.

To ensure grid independency, three sets of grids are evaluated, as presented in Table 3.2. The average Nusselt number for 0.5%CuO-oil nanofluid at Reynolds number Re=750 is calculated. As a conclusion, grid No.3 is considered to be the optimal mesh number which is used in the subsequent simulations.

Table 3.2. Grid independency investigation.

Grid No.	Number of Elements	Average Nusselt Number (CFD)	Average Nusselt Number (EXP) [57]	Variation with Experimental Results %
1	150,800	44.8	43.2	3.7
2	260,600	46.5	45.7	1.7
3	309,400	47.3	47.3	0

3.2. CFD PROCEDURE

Computational fluid dynamics (CFD) is a common tool for studying fluid flow and heat transfer phenomena. The numerical simulation uses a single-phase model to solve the nanofluid flow problem. This model is the simplest one for simulating a nanofluid flow. The following assumptions are employed in this approach:

1. The nanoparticles and the base fluid are assumed to be mixed precisely and the whole mixture is regarded homogeneous. In addition, the fluid phase and solid particles are supposed to be in thermal equilibrium and to flow at the same velocity.

2. Fluid flow that is steady, Newtonian, and incompressible is considered with no thermal or mechanical energy generation.

3. Changes in kinetic and potential energy are considered negligible.

4. No-slip boundary condition is also considered on the walls.

5. The latent energy, which is associated with phase change between the inflow and outflow conditions, is neglected.

The temperature-dependent thermophysical properties of the nanofluid with different nanoparticle volume fractions are introduced by a user-defined function (UDF) by writing a source code in C language and imported into ANSYS fluent. Using the single-phase model, the continuity, momentum, and energy equations are as follows [63]

$$div\left(\rho_{nf}\vec{V}\right) = 0, \tag{3.1}$$

$$div\left(\rho_{nf}\vec{V}\vec{V}\right) = -\nabla P + \mu_{nf}\nabla^2\vec{V}, \tag{3.2}$$

$$div\left(\rho_{nf}\vec{V}C_{P_{nf}}T\right) = div\left(k_{nf}\nabla T\right), \tag{3.3}$$

where $\vec{V}$ and P are the velocity vector and pressure of the flow along the pipe, respectively, ρ_{nf}, μ_{nf}, and k_{nf} are the density, dynamic viscosity, and thermal conductivity.

The discretization method is defined as the approach of approximating the differential equations by a set of algebraic equations for the variables at some set of discrete locations in space and time. The governing equations can be discretized using three main methods as finite difference method, finite volume method, and the finite element method (FVM). The CFD code which has been used in this work using ANSYS Fluent is based on the finite volume method. This method has been very successful in solving fluid flow problems. A finite volume is a numerical approach for solving partial differential equations. These partial differential equations are calculated by the conserved variables averaged values in the control volume.

The finite volume method is used to discretize the governing differential equations, and the semi-implicit technique for pressure-linked equations (SIMPLE) algorithm is used to solve the velocity-pressure coupling. CFD simulations are applied on nanofluid flow utilizing ANSYS FLUENT to solve the governing equations of the flow. The convection and diffusion terms in the governing equations were discretized using a second-order upwind scheme. The convergence criteria of the solutions monitored by a residual monitor of 10^{-6}.

4. NANOFLUID FLOW PROPERTIES

In this chapter, the properties of nanofluid flow will be discussed. The fundamental equations used to analyse the heat transfer and hydrodynamic behaviour of different nanofluid flows are presented. These equations cover parameters such as heat transfer coefficient, Nusselt number, a newly defined Reynolds number specific to nanofluids, pumping power, performance efficiency index, wall shear stress, and friction factor. Additionally, various definitions are provided for different scenarios and boundary conditions.

4.1. FORMULAS USED

The nanofluid flows through a circular horizontal pipe of a length L and diameter D_{in} (see Fig. 3.1) with uniform inlet temperature and velocity distributions are experimentally investigated by Esmaeilzadeh et al. [62]. The same geometry is created using Design Modeler and a three-dimensional flow case is chosen to match the experimental set-up. The flow direction is parallel to the pipe axis and the pipe wall is considered to be completely smooth. The energy transported by the nanofluid flow inside the pipe, which is the heat generated by the DC power supply in the reference experimental paper, is calculated by [57]

$$q_{nf} = \dot{m}_{nf} C_{p_{nf}} \left(T_{nf_{(out)}} - T_{nf_{(in)}} \right), \tag{4.1}$$

where $\dot{m}_{nf}$ is the mass flow rate, $T_{nf_{(out)}}$ and $T_{nf_{(in)}}$ are outlet and inlet temperatures, $C_{p_{nf}}$ is the specific heat capacity.

Heat transfer rate can be expressed by surface heat flux using the below equation as

$$q_{nf} = q''_{nf} A_s, \tag{4.2}$$

where q''_{nf} and A_s are the surface heat flux and the surface area of the pipe wall, respectively. The heat flux is defined as

$$q''_{nf} = -k_{nf} \left(\frac{\partial T}{\partial r} \right)_{r=R}, \tag{4.3}$$

where r represents the radial axis, while R denotes the radius of the pipe.

4.1.1. HEAT TRANSFER

The average convective heat transfer coefficient of the nanofluid flow along the pipe length is defined as

$$h_{nf_{(avg)}} = \frac{1}{L} \int_0^L h_{nf}(x) dx \, , \tag{4.4}$$

where $h_{nf}(x)$ is the local heat transfer coefficient at any axial distance from the pipe inlet determined by

$$h_{nf}(x) = \frac{q''_{nf}}{T_s(x) - T_{b_{nf}}(x)}, \tag{4.5}$$

and $T_s(x)$ is the pipe wall temperature along the pipe length and $T_{b_{nf}}(x)$ is the bulk temperature at any axial distance using the principles of conservation of energy as

$$T_{b_{nf}}(x) = T_{nf_{(in)}} + \frac{q''_{nf} \pi D_{in}}{\dot{m}_{nf} C_{p_{nf}}} x\ . \tag{4.6}$$

The average Nusselt number of the nanofluid flow along the entire length of the pipe is defined as

$$\mathrm{Nu}_{nf_{(avg)}} = \frac{1}{L} \int_0^L \mathrm{Nu}_{nf}(x)\, dx\ , \tag{4.7}$$

where $\mathrm{Nu}_{nf}(x)$ is the local Nusselt number of the nanofluid flow at any given axial distance from the pipe inlet as

$$\mathrm{Nu}_{nf}(x) = \frac{h_{nf}(x) D_{in}}{k_{nf}}. \tag{4.8}$$

4.1.2. REYNOLDS NUMBER OF THE NANOFLUID

Since the single-phase approach is considered, the average velocity for the base fluid and the nanofluid is the same. Using (2.1) and (2.3), the relationship between the Reynolds number ($\mathrm{Re} = \rho VD/\mu$) of the nanofluid and the Reynolds number of the base fluid is expressed as

$$\mathrm{Re}_{nf} = \mathrm{Re}_{bf} \left(\frac{\rho_{nf}}{\rho_{bf}} \frac{\mu_{bf}}{\mu_{nf}} \right). \tag{4.9}$$

The significance of the newly introduced equation lies in its unique contribution to evaluating the impact of nanoparticles on the fundamental dimensionless number, the Reynolds number.

4.1.3. PUMPING POWER

In nanofluid flow within pipes, pumping power is crucial for ensuring efficient system operation and minimizing energy consumption. Nanoparticles added to base fluids alter rheological properties, affecting flow resistance and thus the required pumping power. Understanding this relationship is essential for optimizing system performance. Nanofluids, with their enhanced thermal conductivity, offer promising opportunities for improved heat transfer in various applications. Managing pumping power effectively enables the realization of nanofluid technology's full potential, facilitating more efficient and sustainable thermal management solutions across industries. The pumping power required to pump the nanofluid into the pipe is calculated as follows [34]

$$\dot{W}_{nf} = \dot{V}_{nf} \Delta P_{nf}, \tag{4.10}$$

where $\dot{V}_{nf}$ is the volume flow rate of nanofluid in the pipe, and ΔP_{nf} is the pressure drop along the pipe.

4.1.4. PERFORMANCE EFFICIENCY INDEX (PEI)

The performance efficiency index is a measure used to evaluate the effectiveness of incorporating nanoparticles into base fluids. By considering factors like heat transfer enhancement and pressure drop ratios, the performance efficiency index quantifies the overall impact of adding nanoparticles. It considers the increased thermal conductivity and heat transfer coefficient due to nanoparticles, as well as the potential rise in pressure drop caused by their presence. A performance efficiency index greater than one is generally indicative of reasonable efficiency when utilizing nanofluids and base fluids. The performance efficiency index is given by [49]

$$\mathrm{PEI} = \frac{\mathrm{Nu}_{nf}}{\mathrm{Nu}_{bf}} \left(\frac{f_{nf}}{f_{bf}}\right)^{-1/3}, \tag{4.11}$$

where f_{nf} and f_{bf} represent the friction factors for the nanofluid and the base fluid, respectively.

4.1.5. WALL SHEAR STRESS AND FRICTION FACTOR

In nanofluid flow within pipes, wall shear stress, friction factor, and skin friction coefficient are crucial parameters governing fluid dynamics and energy losses. As nanoparticles are introduced into the base fluid, they alter the flow behavior, impacting the distribution of shear stress along the pipe wall. The friction factor and skin friction coefficient quantify the resistance encountered by the fluid as it flows through the pipe, reflecting the energy dissipation due to viscous effects. Accurate characterization of these parameters is essential for optimizing system design and predicting pressure drop in nanofluid-based systems, thereby facilitating efficient heat transfer and fluid transport applications.

The wall shear stress of the nanofluid flow along the pipe is defined as

$$\tau_{w_{nf}} = \mu_{nf} \left(\frac{\partial u}{\partial r}\right)_{r=R}. \tag{4.12}$$

The friction factor for the hydrodynamically fully developed region of the pipe is given by [35]

$$f_{nf} = \frac{8\tau_{w_{nf}}}{\rho_{nf} V_{nf_{(avg)}}^{2}}, \tag{4.13}$$

where $V_{nf_{(avg)}}$ is the average nanofluid flow velocity in the pipe.

The theoretical friction factor for the hydrodynamically fully developed laminar flow is given by [64]

$$f_{bf} = \frac{64}{\mathrm{Re}}. \tag{4.14}$$

The skin friction coefficient is defined as

$$C_{f_{nf}} = \frac{\tau_{w_{nf}}}{\rho_{nf} V_{nf_{(avg)}}{}^{2}} . \tag{4.15}$$

4.1.6. α INDEX CRITERION DEFINITION

In the case of laminar flow, the evaluation of heat transfer efficiency can be measured by parameter α as the ratio of the relative increase in nanofluid's viscosity to the relative enhancement in nanofluid's thermal conductivity as given [65]

$$\alpha = \left(\frac{\mu_{nf}}{\mu_{bf}} - 1\right) / \left(\frac{k_{nf}}{k_{bf}} - 1\right) . \tag{4.16}$$

For heat transfer purposes, using nanofluids instead of base fluids is advantageous if $\alpha < 4$ [65].

4.1.7. THERMAL BOUNDARY LAYER THICKNESS

Due to the variation in temperature between the inner wall of the pipe and the bulk fluid flowing inside the pipe, convective heat transfer takes place, forming a thermal boundary layer. Thus, the impact of heat transfer extends further into the center of the pipe and the thermal boundary layer grows. The thermal boundary layer thickness $\delta_t(x)$ at any given axial distance 'x' from the pipe entrance is defined as the value of radius 'r' at which the following relationship is met [66]

$$\delta_t(x) = \frac{T_s(x) - T(x,r)}{T_s(x) - T_m(x)} = 0.99 , \tag{4.17}$$

where $T(x, r)$ is the nanofluid local temperature inside the pipe space.

The average thickness of thermal boundary layer along the pipe length can be calculated as

$$\overline{\delta_t} = \frac{1}{L} \int_0^L \delta_t(x) dx . \tag{4.18}$$

4.2. THE BOUNDARY CONDITIONS

For the case of Al_2O_3-water nanofluid: Numerical simulations were performed on the hydrodynamic and heat transfer characteristics of the three-dimensional flow of Al_2O_3-water nanofluid for horizontal circular tube flow. The flow is incompressible, steady-state, with a constant and uniform heat flux along the tube surface under boundary conditions. The nanofluid is considered with both constant and temperature-dependent thermophysical properties with volume fractions between 0.1% and 5%. The simulations were carried out using the single-phase Newtonian model with Reynolds numbers between 310 and 1950. The Nusselt number and the heat transfer coefficient in the tube are investigated simultaneously in the developing and hydrodynamically developed regions. A crucial factor in predicting flow and heat transfer characteristics of Al_2O_3-water nanofluids is to accurately determine the effect of nanoparticle volume fraction on the hydrodynamic and thermal entry lengths. The hydrodynamical and thermal characteristics of Al_2O_3-water nanofluid laminar pipe flow using Computational Fluid Dynamics (CFD) method are investigated. The impact of adding nanoparticles to the base fluid on Nusselt number, heat transfer coefficient, the thermal and hydrodynamic entry length is examined at different Reynolds numbers. According to my knowledge, no analytical or numerical expressions have been identified to represent the development length for nanofluid flows. Based on the simulation results, two correlations have been suggested for the calculation of the hydrodynamic and thermal entry length for Al_2O_3-water nanofluid laminar pipe flow. A constant and uniform surface heat flux $q''_{nf} = q_{nf}/\pi D_{in} L$ is applied on the wall as $9000\ W/m^2$. The inlet temperature of the nanofluid flow is kept at constant $T_{nf_{(in)}} = 298.15K$. At the inlet section: $X = 0, u = U_{in}$, and $T = T_{in}$, are used as inlet velocity and temperature conditions. At the outlet section: A fully developed condition is assumed at the outlet, and all derivatives are taken as zero. i.e., $X = L$, $\frac{\partial u}{\partial x} = \frac{\partial v}{\partial x} = \frac{\partial w}{\partial x} = \frac{\partial T}{\partial x} = 0$, $\vec{V} = (u, v, w)$. On the pipe wall: no-slip conditions, $u = v = w = 0$, and constant heat fux (9000W m^{-2}) are imposed.

For the case of CuO-water nanofluid: The velocity distribution and heat transfer improvement in a two-dimensional channel filled with a Cuo–water nanofluid is numerically studied. The nanofluid flow is assumed laminar and single-phase with Newtonian behaviour. Pure water is considered as the base fluid, and Cuo–water nanofluid with four different volume fractions of CuO nanoparticles are examined. The effects of nanoparticle volume fraction on the heat transfer, velocity profile, wall shear stress, skin friction coefficient, and Nusselt number along the channel have been examined. A constant heat source–sink is considered to cover the entire length of the bottom wall of the channel while the upper wall is assumed thermally insulated. The channel's diameter and length have been set at 0.1m and 2m, respectively. With a temperature of $275K$ and a velocity given by Reynolds numbers equal to 1000 (Re=1000), the flow at the inlet has been assumed to be hydrodynamically steady. The lower wall receives a constant heat flux of 200 W/m^2 from downside, while the upper wall is set to be adiabatic from up (see Fig. 3.4).

For the case of CuO:MWCNT-Oil hybrid nanofluid: There have been limited studies on the improvement of heat transfer resulting from hybrid oil nanofluids. The three-dimensional steady-state flow of CuO and MWCNT nanoparticles in engine oil within a horizontal pipe is performed. The simulations are investigated for various volume fractions of the nanoparticles while maintaining a constant heat flux boundary condition on the pipe wall. The purpose of the research is to compare the impact of concentrations of CuO and MWCNT nanoparticles mixed at different ratios on convective heat transfer. The effect of changing the volume fractions of nanoparticles (CuO and MWCNT) on the convective heat transfer coefficient and the Nusselt number is analysed in the simulations at Reynolds number Re=750. The numerical studies were carried out with uniform temperature and velocity profiles at the inlet of the horizontal pipeline. The direction of the flow was defined normal to the boundary. The inner surface of the pipe wall was assumed to be perfectly smooth with zero roughness height. The surface heat flux is taken as $208756\ W/m^2$ in the calculations. The mean temperature of the engine oil as a base fluid inside the test section increased from $303.15\ K$ to $333.15\ K$ because of constant heat flux. Reynolds number is 750. All thermophysical properties of the engine oil are evaluated at the average temperature, $T_{avg} = 318.5\ K$. The impact of nanoparticle volume fractions as well as nanoparticle volume ratios on convection heat transfer overall performance is studied. To this aim, it is worthwhile to consider several parameters including heat transfer coefficient, Nusselt number, thermal boundary layer thickness, temperature profile, and velocity profile along the pipe. The thermal boundary layer profiles along the pipe for the examined nanofluids are plotted accurately. The results from the comparison of thermal boundary layer thickness, temperature, and velocity profiles for all nanofluids are shown in graphical form. A scale analysis is also conducted to identify the correlation between the thermal boundary layer thickness and heat transfer coefficient.

Comparative Analysis of Water-Based Nanofluids: AL_2O_3, CuO, TiO_2, and Ag: Numerical simulations on the 3D steady-state laminar flow of different water-based nanofluids in a horizontal pipe are conducted using the single-phase model considering temperature-dependent thermophysical properties. The simulations are performed to compare the heat transfer performance and hydrodynamic behaviour for nanofluids including Al_2O_3, CuO, TiO_2, and Ag nanoparticles under constant heat flux boundary condition on the pipe wall. Nanoparticle volume fractions ranging from 0.5% to 3% were examined at Reynolds numbers ranging from 310 to 1950. Key parameters such as Nusselt number, heat transfer coefficient, pressure drop, and pumping power were analysed. Single-phase CFD approach for solving the flow of nanofluid problem is employed. The flow is assumed to be steady, Newtonian, and incompressible. The nanofluid flows through a circular horizontal pipe of a length L=1m and diameter D_{in}=7 mm with a constant and uniform inlet temperature and velocity distribution as experimentally investigated by Esmaeilzadeh [62]. The constant and uniform surface heat flux is applied on the wall as $9000\, W/m^2$. The inlet flow temperature is constant $T_{in} = 298.15K$. The geometry is created using Design Modeler and a three-dimensional flow case is chosen to match the experimental set-up. The convergence criteria of the solutions were considered by a residual value of 10^{-6}. To analyse grid independency, the local heat transfer coefficient for water and Al_2O_3-water nanofluid at Re=1300 for a wide range of mesh sizes are investigated and compared with the experimental results [62]. The mesh with 830415 elements has been selected and will be used in further simulations.

5. RESULTS AND DISCUSSION

This chapter focuses on analysing and validating simulation results for different nanofluids. It examines various factors such as constant versus temperature-dependent thermophysical properties, hydrodynamic and thermal entry lengths, heat transfer and hydrodynamic performance, thermal boundary layer thickness, and the performance efficiency index (PEI). The aim is to provide a comprehensive understanding of the simulated system's behaviour and performance characteristics.

5.1. VALIDATION OF THE SIMULATION RESULTS

The Nusselt number for pure water (as the base fluid) along the pipe length for constant and temperature-dependent thermophysical properties at Re=799.53 is compared with the experimental results conducted by Esmaeilzadeh et al. [62] and the correlations suggested by Shah [3] and Grigull [67] and Churchill and Ozoe [68] (see Fig. 5.1). The correlation of Shah and Grigull for the developing region of the pipe flow with constant wall heat flux is given as

If $x^* < 5.10^{-5}$

$$\mathrm{Nu}(x^*) = \frac{1.302}{(x^*)^{\frac{1}{3}}} - 1 \ , \tag{5.1}$$

If $5.10^{-5} \leq x^* < 1.5.10^{-3}$

$$\mathrm{Nu}(x^*) = \frac{1.302}{(x^*)^{\frac{1}{3}}} - 0.5 \ \ , \tag{5.2}$$

If $x^* \geq 1.5.10^{-3}$

$$\mathrm{Nu}(x^*) = 4.364 + \frac{8.68\, e^{-41x^*}}{(10^3 x^*)^{0.506}} \ \ , \tag{5.3}$$

where the non-dimensional axial distance is $x^* = \frac{x}{D_{in}\ \mathrm{Re\ Pr}}$ and $\mathrm{Pr} = \mu C_p/k$ is the Prandtl number.

The correlation provided by Churchill and Ozoe [68] for the entry and fully developed regions of the pipe flow for the base fluid with constant wall heat flux is given as

$$\mathrm{Nu}(x) = 5.364\left(1+\left(\frac{\mathrm{Gz}}{55}\right)^{\frac{10}{9}}\right)^{\frac{3}{10}}\left[1+\left[\frac{\mathrm{Gz}}{28.8}\left(1+\left(\frac{\mathrm{Pr}}{0.0207}\right)^{\frac{2}{3}}\right)^{-\frac{1}{2}}\left(1+\left(\frac{\mathrm{Gz}}{55}\right)^{\frac{10}{9}}\right)^{-\frac{3}{5}}\right]^{\frac{5}{4}}\right]^{\frac{2}{5}} - 1\ , \tag{5.4}$$

where $\mathrm{Gz} = \pi/4x^*$ is the Graetz number. The simulation results are compared with experimental data obtained using temperature-dependent and constant thermophysical properties. The analysis revealed that the simulations using temperature-dependent thermophysical properties are in a good agreement with the experimental data, particularly for values of x/D above 40, with an average discrepancy of 2.39%. The simulations using constant thermophysical properties provided a higher average discrepancy of 4.35%. These results suggest that the incorporation of temperature-dependent thermophysical properties significantly improves the accuracy of simulations compared to constant thermophysical properties.

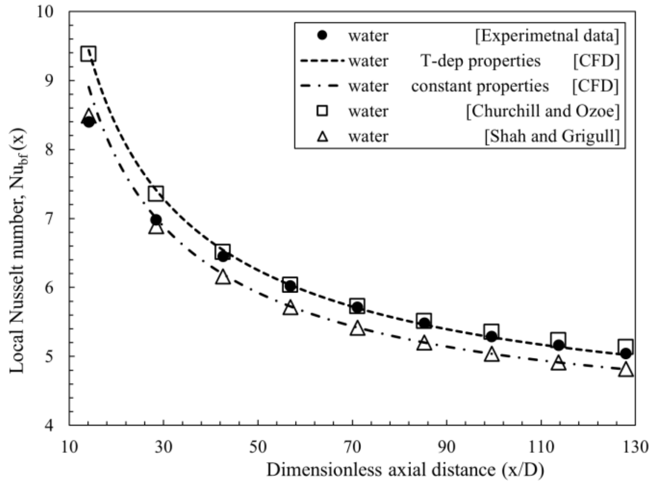

Fig. 5.1. Validation of the CFD results with experimental data for constant and temperature-dependent thermophysical properties.

Note that the CFD results obtained using temperature-dependent thermophysical properties also agreed well with the Churchill and Ozoe correlation (5.4), with an average error of 0.94%. On the other hand, the CFD results using constant thermophysical properties exhibited good agreement with the Shah and Grigull correlations (5.1)-(5.3), with an average error of 0.81%.

The proposed model is applied in the simulations in order to evaluate the heat transfer performance of CuO:MWCNT-oil nanofluid in pipe flow. To do this, first it is necessary to assure the validity of the model. In Fig. 5.2, the simulation results for local Nusselt number along the pipe length for CuO-oil nanofluid with volume fractions of 0.1, 0.2, and 0.5% are compared with the experimental results [57]. The average and maximum differences between the simulation results and experimental data are 2.8% and 5.6%, respectively.

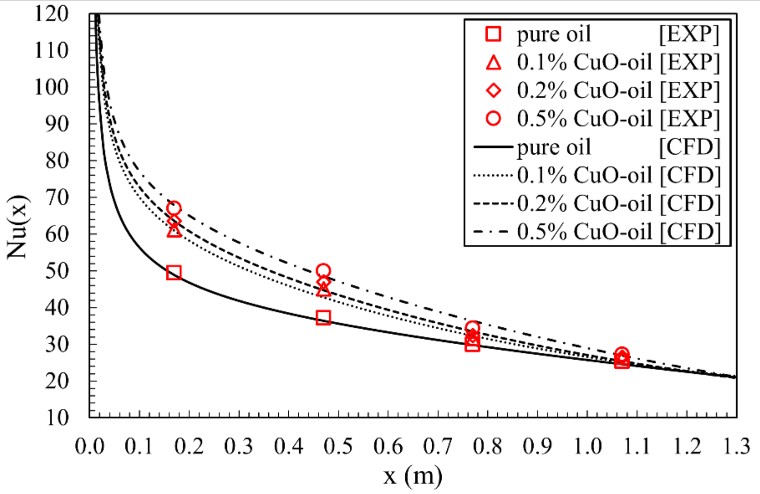

Fig. 5.2. Comparison between simulation and experimental results for CuO-oil nanofluid at Re = 750.

It confirms that the simulation of the present model can also predict the heat transfer performance of CuO:MWCNT-oil nanofluid within the acceptable range of accuracy.

In order to validate the numerical solver, the simulation results of Nusselt number for the nanofluid containing 0.4% CuO were compared to the findings of the experimental study conducted by Heris et al. [57] (see Fig. 5.3). The results of the simulation exhibited a good agreement with the experimental findings. Changes in the average Nusselt number against the Reynolds number at different nanoparticle volume fractions are depicted in Fig. 5.4.

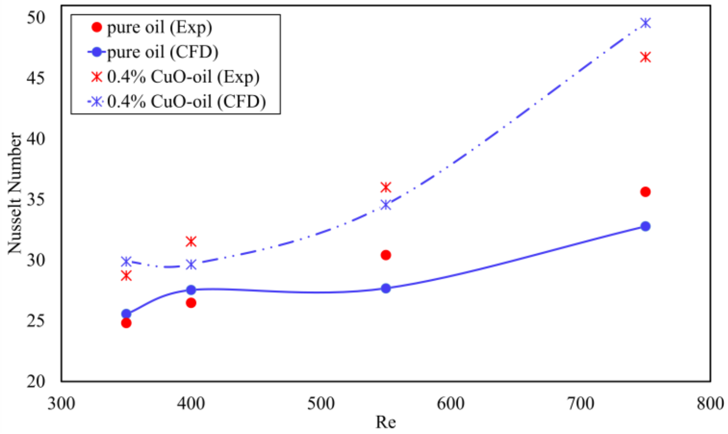

Fig. 5.3. Comparison between the Nusselt number obtained from the CFD and experiment for pure oil and CuO 0.4%-oil.

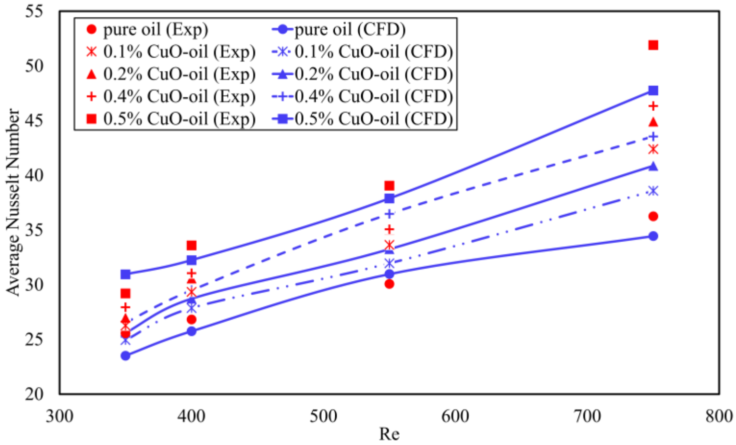

Fig. 5.4. Average Nusselt number variation against Reynolds number for nanofluid in different volume fractions.

It can be seen from Fig. 5.4, that the Nusselt number increased significantly as the nanoparticle volume fraction and the Reynolds number increased. Figure 5.5 shows the variation of the local heat transfer coefficient along the axial direction of the pipe for nanofluid at a Reynolds number of about 750. The CFD results showed a good agreement with the experimental data.

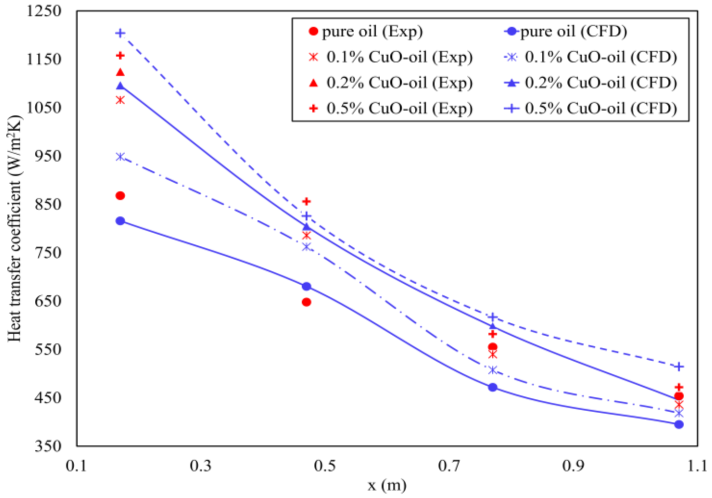

Fig. 5.5. Variation of local heat transfer coefficient along the axial direction of pipe for nanofluid at a Re=750.

The friction factor of the nanofluids with different volume fractions has the same value. Note that using a single-phase approach, the friction factor only depends on the Reynolds number. In Fig. 5.6, the friction factor of water in the hydrodynamically fully developed region of a pipe was evaluated for Reynolds numbers ranging from 310 to 1950. My analysis showed that the CFD results gave a relatively small average deviation of 4.19% compared to the experimental data [62] and CFD results showed good agreement with theoretical values, with an average deviation of 0.13%. These results suggest that the simulations can be effectively used to predict the friction coefficient in single-phase laminar flow in a circular horizontal pipe.

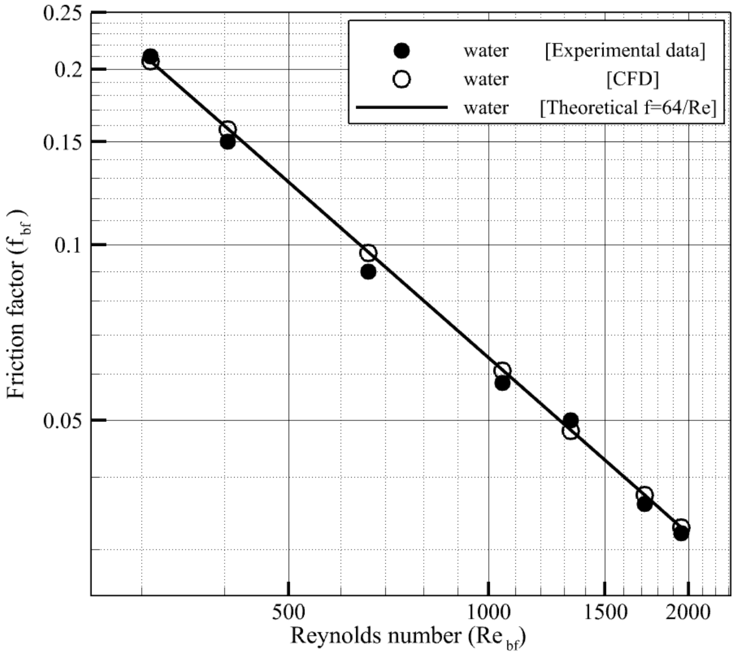

Fig. 5.6. Validation of the friction factor of water at different Reynolds numbers.

5.2. CONSTANT VERSUS TEMPERATURE-DEPENDENT THERMOPHYSICAL PROPERTIES

The accuracy of the simulations for the local heat transfer coefficient of the water and Al_2O_3-water nanofluid was examined and the CFD results were obtained using constant and temperature-dependent thermophysical properties, with nanoparticle volume fractions of 0.5% and 1%. These results were compared with experimental data in Ref. [62] at Re=1300 (see Fig. 5.7).

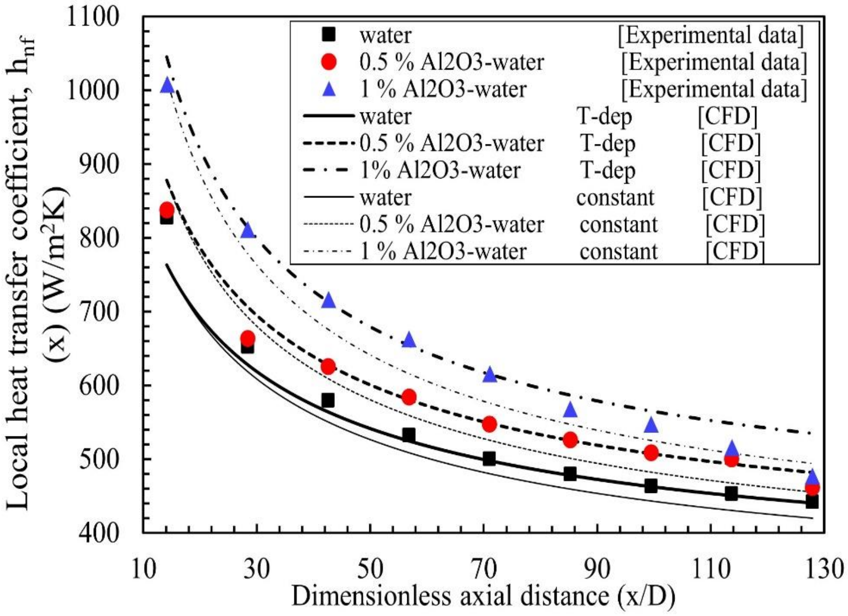

Fig. 5.7. Validation of the CFD results for $h_{nf}(x)$ for constant and temperature-dependent thermophysical properties.

Figure 5.7 shows that the CFD results for $h_{nf}(x)$ at $\mathrm{Re}_{nf} = 1300$ using temperature-dependent thermophysical properties presented good agreement with the experimental data, with an average error of 2.44%, but the constant thermophysical properties give a higher average error of 4.44%. These results suggest that considering temperature-dependent thermophysical properties can significantly improve the accuracy of simulations. It was also observed that an increase in nanoparticle concentration was associated with an increase in the heat transfer coefficient, regardless of whether the fluid properties were constant or variable.

Figure 5.8 demonstrates the local heat transfer coefficients along the pipe for nanofluid with volume fraction of 0.5% and 1% at Reynolds number 799.53 for constant and temperature-dependent thermophysical properties. The local heat transfer coefficients show an increasing trend with increasing the nanoparticle concentration for both constant and temperature-dependent thermophysical properties. The heat transfer coefficients decline with the axial distance because the temperature gap between the fluid near the wall and the bulk fluid becomes greater along the pipe length. Moreover, when considering temperature-dependent thermophysical properties, the local heat transfer coefficients demonstrate higher values compared to constant properties.

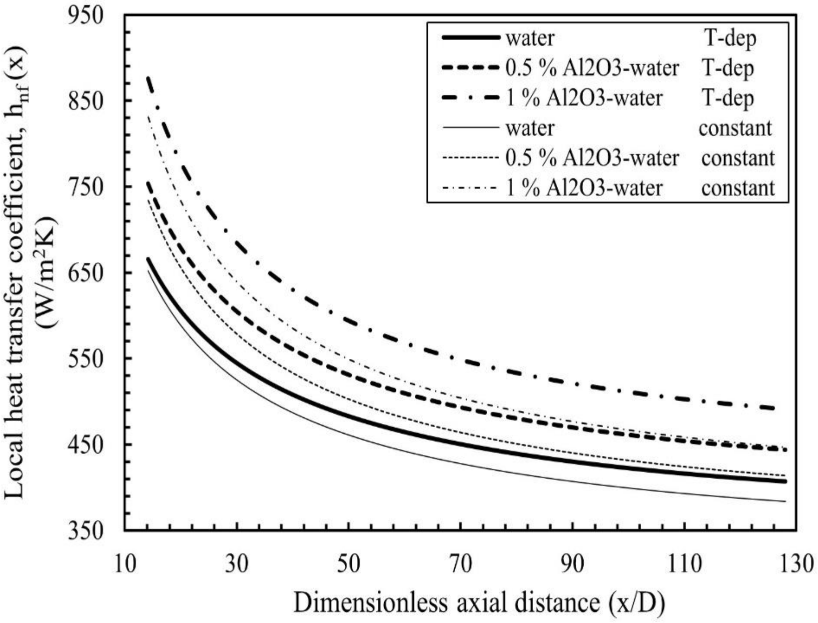

Fig. 5.8. Variation of $h_{nf}(x)$ with φ and *(x/D)*.

The average differences in heat transfer coefficients between temperature-dependent and constant properties are 5.1%, 6%, and 8.44% for water, 0.5% Al_2O_3-water nanofluid, and 1% Al_2O_3-water nanofluid, respectively. Furthermore, as the axial distance (x/D) increases, the discrepancy between heat transfer coefficients for temperature-dependent and constant properties also increases. For example, for water, the difference is 2.1% at x/D=14.21 and 6.2% at x/D=127.93. Similarly, for 0.5% Al_2O_3-water nanofluid, the difference is 2.7% at x/D=14.21 and 7.3% at x/D=127.93, and for 1% Al_2O_3-water nanofluid, the difference is 5.4% at x/D=14.21 and 9.8% at x/D=127.93.

Figure 5.9 illustrates the impact of the volume fraction on the local Nusselt number for water and nanofluid with 0.5% and 1% volume fractions for constant and variable thermophysical properties at Re_{nf}=1300. The temperature-dependent thermo-physical properties yield higher results compared to constant properties. In the case of variable properties, the Nusselt numbers exhibit an increase as the volume fraction increases, while the Nusselt numbers for constant properties demonstrate a decrease with increasing volume fraction.

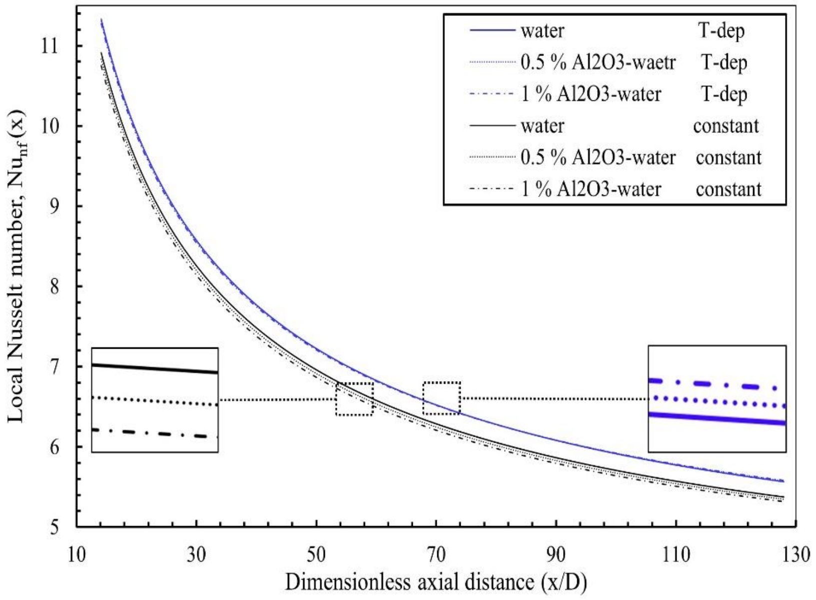

Fig. 5.9. Comparison of the local Nusselt number of the nanofluid for constant and temperature-dependent thermophysical properties.

In Fig. 5.10, the variations of the local Nusselt numbers with *x/D* are compared for constant and temperature-dependent thermophysical properties, in particular for two different Reynolds numbers: 799.53 and 1300. The results show that the increased volume fraction of nanoparticles leads to an increase in the Nusselt number for variable properties and a decrease in constant properties. Furthermore, the Nusselt number is generally higher for variable properties than for constant properties. Figure 5.10 also indicates that the discrepancy between the Nusselt numbers of variable properties and constant properties decreases at higher Re.

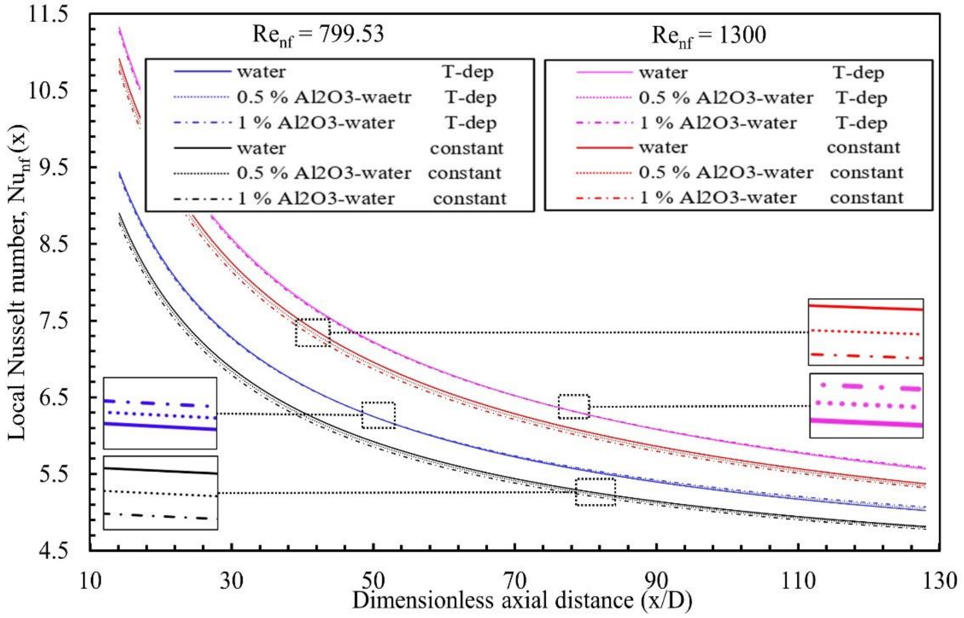

Fig. 5.10. Comparison of the local Nusselt number of the nanofluid for constant and temperature-dependent thermophysical properties.

5.3. α INDEX CRITERION FOR CUO-OIL, MWCNT-OIL, AND CUO:MWCNT-OIL

In Fig. 5.11, the results for α index criterion for nanofluids including CuO-oil, MWCNT-oil, CuO:MWCNT-oil 1:1, and CuO:MWCNT-oil 1:2 are presented. These nanofluids can be considered advantageous over base fluid because they have α index much less than four in the range of nanoparticle volume fractions from 0 to 3%.

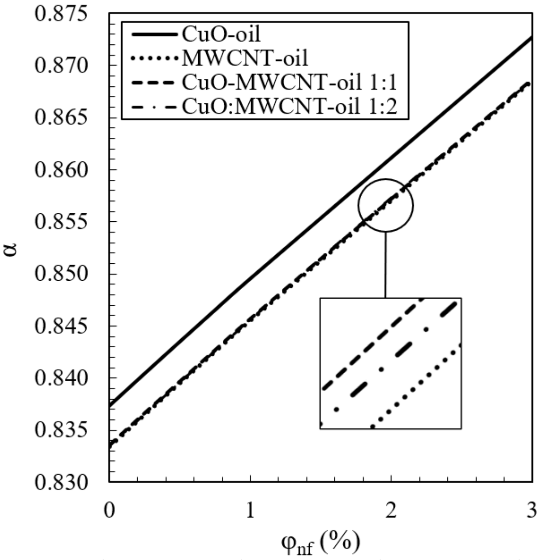

Fig. 5.11. α index for different nanofluids.

5.4. HYDRODYNAMIC AND THERMAL ENTRY LENGTHS

The hydrodynamic and thermal entry lengths are the distances required for the flow velocity to reach fully developed region and the temperature profile to become uniform. A crucial factor in predicting flow and heat transfer characteristics is to accurately determine the effect of nanoparticle volume fraction on the hydrodynamic and thermal entry lengths of nanofluids. The equation of Reynolds number for the nanofluids (Eq.4.9) is particularly valuable in the investigations, where the focus is on the understanding of nanofluid's behavior across a range of Reynolds numbers (310 to 1950), and simultaneously considering the corresponding Reynolds numbers of the base fluid (312 to 2247).

5.4.1. HYDRODYNAMIC ENTRY LENGTH FOR NANOFLUID FLOW

The CFD results on the hydrodynamic entry length for the Al_2O_3-water nanofluid using temperature-dependent thermophysical properties are depicted in Fig. 5.12. It shows that the hydrodynamic entry length for the nanofluids increases linearly with the Reynolds number of the base fluid within the examined range and volume fractions between 0.1% and 5%. Results also confirm that the hydrodynamic entry length decreases with increasing the nanoparticle volume fraction due to the increasing viscosity.

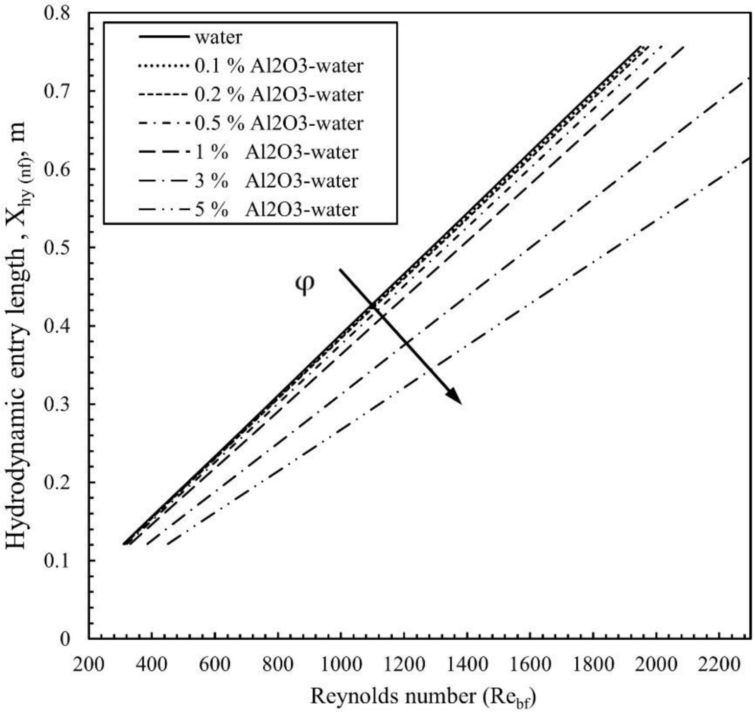

Fig. 5.12. Variation of the $X_{hy_{(nf)}}$ with Re at different volume fractions.

Based on simulations, a novel correlation is suggested to determine the laminar hydrodynamic entry length for the Al_2O_3-water nanofluid for volume fractions ranging from 0.1% to 5% as

$$X_{hy_{(nf)}} = 0.0554\,\mathrm{Re}_{nf}\,D_{in} = 0.0554\,\mathrm{Re}_{bf}\,A(\varphi,T)\,D_{in}, \tag{5.5}$$

$$A(\varphi,T) = \frac{1+(a-1)\varphi}{1+9.4974\varphi+77.811\varphi^2+0.9514\varphi^3}, \tag{5.6}$$

with $a(\varphi,T) = \frac{\rho_{np}}{\rho_{bf}}$, $0.001 \le \varphi \le 0.05$, $310 < \mathrm{Re}_{nf} < 1950$.

For constant thermophysical properties (see Table 2.1), one can get

$$A(\varphi) = \frac{1+2.6562\,\varphi}{1+9.4974\varphi+77.811\varphi^2+0.9514\varphi^3}. \tag{5.7}$$

Note that if the above correlation is used for calculating the hydrodynamic entry length for the base fluid ($\varphi = 0$), the above correlation reduces to $X_{hy_{(bf)}} = 0.0554\,\mathrm{Re}_{bf}$, which agrees well with the correlation suggested by Nguyen et al. [41].

5.4.2. THERMAL ENTRY LENGTH FOR NANOFLUID FLOW

In Fig. 5.13, the relationship between thermal entry length and Reynolds number is illustrated at various volume fractions. The results demonstrate that both the Reynolds number and volume fraction have a direct impact on the thermal entry length. As the Reynolds number increases, the thermal entry length increases linearly for a given volume fraction. The thermal entry length also increases with increasing the volume fraction at a given Reynolds number. However, the effect of the volume fraction is more significant at higher Re. This observation suggests that the addition of nanoparticles to the base fluid results in the flow reaching thermally fully developed states at a larger axial distance from the inlet. Consequently, the convective heat transfer within the pipe intensifies along the entry section, significantly influencing the overall heat transfer rate.

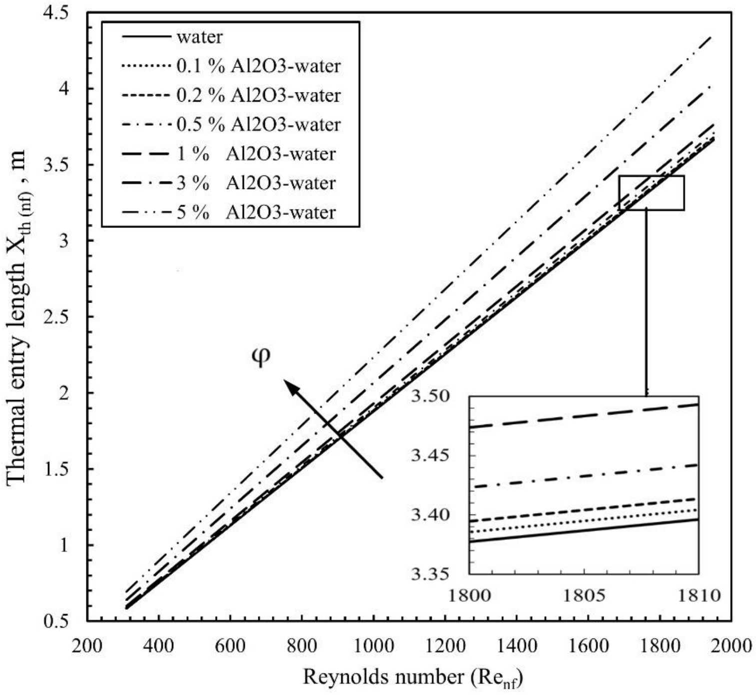

Fig. 5.13. Variation of the $X_{th(nf)}$ with Re and φ.

In Fig. 5.14, the relationship between the thermal entry length and volume fraction is depicted. The range of Reynolds number is from 310 to 1950 and the range of volume fraction is from 0.1% to 5%. The findings demonstrate a clear increase in the thermal entry length as volume fraction increases. The addition of nanoparticles to the base fluid enhanced the heat transfer rate. The increase in the thermal entry length is higher at higher Reynolds numbers.

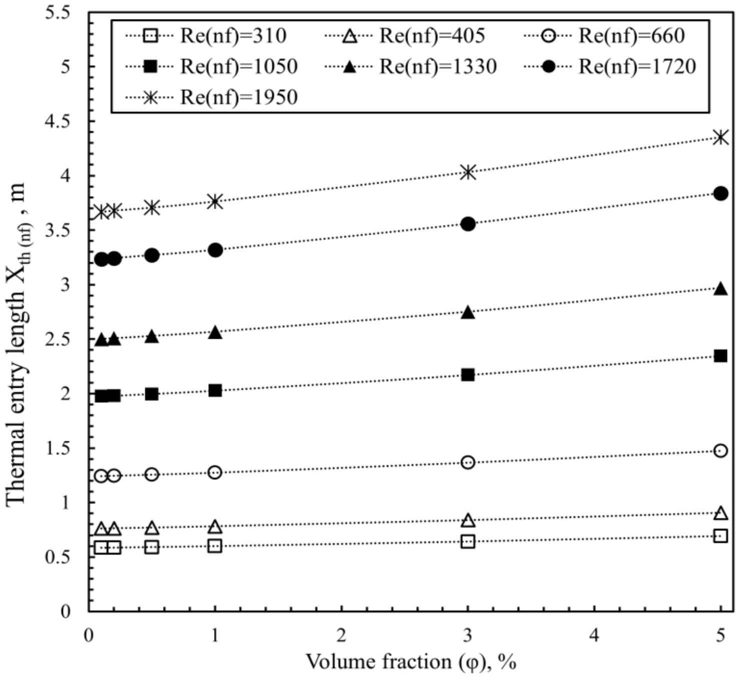

Fig. 5.14 Variation of $X_{th(nf)}$ with φ and Re.

Based on the CFD results, I introduce a new correlation to calculate the laminar thermal entry length of the Al_2O_3-water nanofluid flow in a horizontal pipe as

$$X_{th(nf)} =$$

$$\left(0.043 - \frac{4.823\varphi}{10^6}\right)\mathrm{Re}_{nf}\mathrm{Pr}_{nf}D_{in} =$$

$$\left(0.043 - \frac{4.823\varphi}{10^6}\right)\mathrm{A}(\varphi,T)\mathrm{B}(\varphi,T)\mathrm{Re}_{bf}\mathrm{Pr}_{bf}D_{in}, \tag{5.8}$$

$$\mathrm{B}(\varphi,T) = (1 + 9.4974\varphi + 77.811\varphi^2 + 0.9514\varphi^3)\,\frac{\frac{1-\varphi}{1-\varphi+a\varphi}+ab\varphi}{1+\frac{3(c-1)\beta^3\varphi}{c+2-(c-1)\beta^3\varphi}}, \tag{5.9}$$

with $b(\varphi,T) = \frac{C_{p_{np}}}{C_{p_{bf}}}$, $c(\varphi,T)=\frac{k_{np}}{k_{bf}}$, $0.1\% < \varphi < 5\%$, $310 < \mathrm{Re}_{nf} < 1950$,

where the nanofluid Prandtl number is defined as $\mathrm{Pr}_{nf} = \mu_{nf}C_{p_{nf}}/k_{nf}$.

Applying constant thermophysical properties I get

$$\mathrm{B}(\varphi) = (1 + 9.4974\varphi + 77.811\varphi^2 + 0.9514\varphi^3)\,\frac{\frac{1-\varphi}{1+2.6562\varphi}+0.6688\varphi}{1+\frac{262.2070\varphi}{68.6667-87.4023\varphi}}. \tag{5.10}$$

The thermal entry length increases linearly with the Reynolds number at constant volume fraction (see Fig. 5.13). The thermal entry length increases also linearly with the volume fraction at a constant Re (see Fig. 5.14). If $\varphi = 0$, the correlation can predict the thermal entry length for water, which agrees with the Pagliarini's correlation [32] for the thermal entry length of the base fluid as $X_{th_{(bf)}} = 0.043\ \mathrm{Re}_{bf}\ \mathrm{Pr}_{bf}\ D_{in}$.

5.5. HEAT TRANSFER PERFORMANCE

In this section, heat transfer performance for different nanofluids is analyzed and temperature contours, temperature profiles, heat transfer coefficients, and Nusselt numbers are investigated and compared.

5.5.1. TEMPERATURE CONTOUR

The temperature contour for CuO-water nanofluid containing 4% CuO along the whole 2D channel is presented in Fig. 5.15. As it is illustrated, the nanofluid enters the channel at temperature equal to inlet temperature ($275K$), and the temperature gradually increases as it moves forward along the channel. Due to having a constant heat flux at the lower wall while the upper wall is thermally insulated, the temperature of nanofluid at lower part of the channel specifically near to the lower wall tends to rise. To precisely investigate the thermal behavior of nanofluid, three cross sections along the channel (X=0.1, 0.5, and 2 m) are selected.

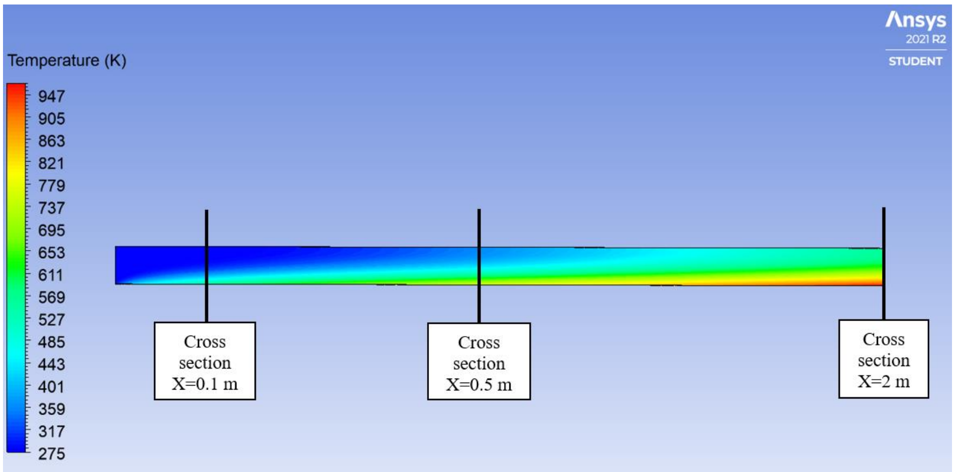

Fig. 5.15. Temperature contour for nanofluid containing 4% CuO along the pipe.

5.5.2. TEMPERATURE PROFILES

Numerical results for CuO-water nanofluid flow for the thermal boundary layers at different locations along the 2D channel are presented. Figure 5.16 depicts the impact of nanoparticle volume fraction on the temperature profile for CuO-water nanofluid flow at three different cross sections (X=0.1, 0.5, and 2 m) along the channel. The Y-axis shows diameter of the channel while the X-axis shows temperature. Thermal boundary layer thickness increases with an increase in the parameter φ which is nanoparticle volume fraction. Comparison of the temperature profiles for different nanofluid concentrations shows that CuO-water at 4% has the thickest thermal boundary layer. Therefore, it is observed that the nanoparticles change the flow and heat transfer characteristics and causes an increase in the thermal boundary layer. Moreover, the graph shows that the temperature near the lower wall at cross section X=0.1m is around 475*K* while it rises to 650*K* and 950*K* at cross sections X=0.5m and X=2m, respectively. This is due to existence of a constant heat flux at the bottom wall along the channel when the nanofluid reaches the end of the channel, it receives more heat from the lower wall. However, the increase of temperature near the upper wall along the channel length is not as rapid as that of for the lower wall since the upper wall is thermally insulated and is receiving heat only from the nanofluid flowing inside the channel.

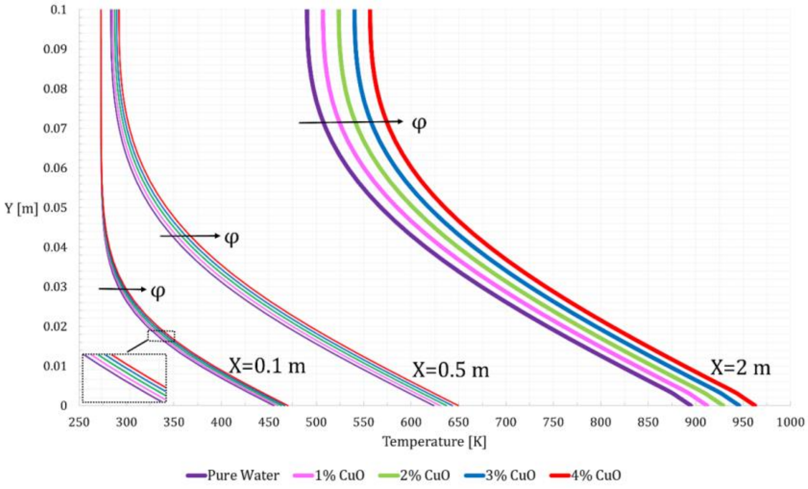

Fig. 5.16. Temperature distribution at different cross sections for different nanoparticle volume fractions

Temperature profiles for the base fluid (oil) and CuO-oil and CuO:MWCNT-oil nanofluids with different nanoparticle volume fractions at three cross sectional areas along the pipe are depicted in Figs. (5.17)-(5.19). T.B.L, which stands for thermal boundary layer, represents the length of ‘r’ adjacent to the wall in which all the thermal boundary layers are being formed. As it can be seen, temperature profile outgrows with increasing nanoparticle volume fraction suggesting that heat penetrates further into the mainstream towards the center of the pipe. However, temperature profiles for 2%CuO-oil nanofluid and 3%CuO-oil nanofluid outgrow temperature profiles for 1%CuO:1%MWCNT-oil hybrid nanofluid and 1%CuO:2%MWCNT-oil hybrid nanofluid, respectively, due to the fact that 2%CuO-oil nanofluid and 3%CuO-oil nanofluid have lower Prandtl numbers (see Table 5.3), and consequently, heat can transfer further into the mainstream.

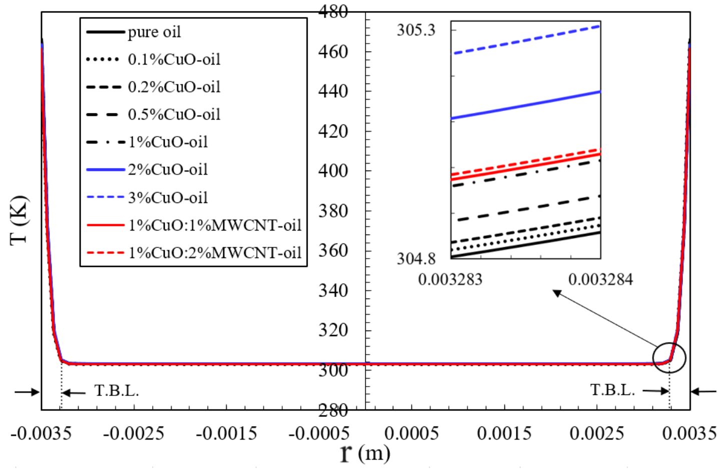

Fig. 5.17. Temperature profiles for the base fluid and nanofluids at *x*=0.02m.

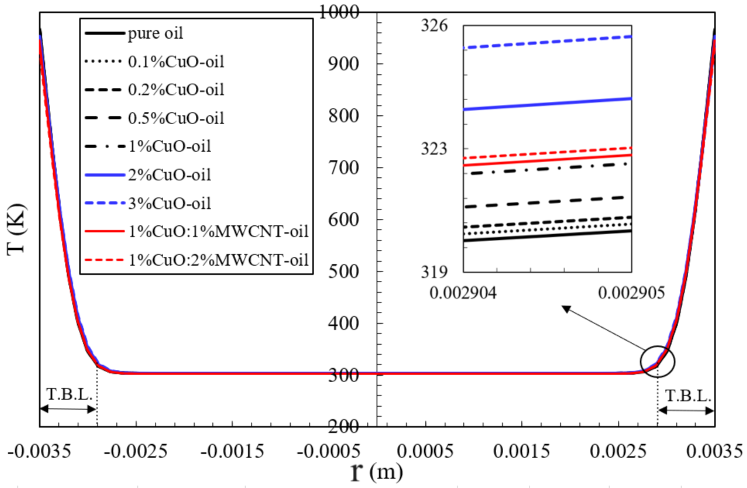

Fig. 5.18. Temperature profiles for the base fluid and nanofluids at *x*=0.65m.

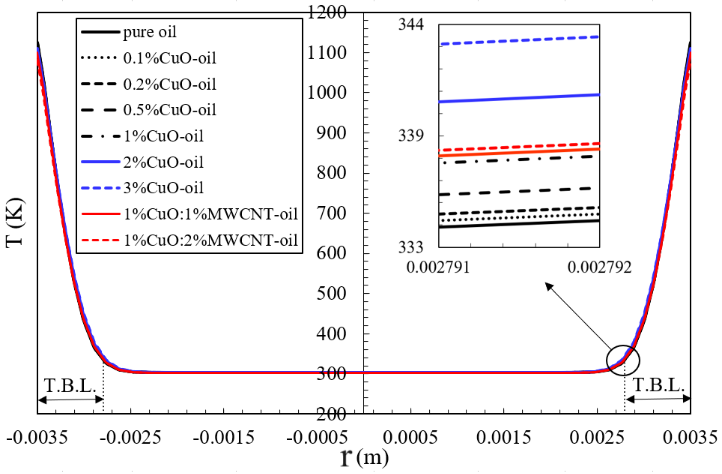

Fig. 5.19. Temperature profiles for the base fluid and nanofluids at *x*=1.3m.

5.5.3. HEAT TRANSFER COEFFICIENT AND NUSSELT NUMBER

Simulation results for local Nusselt number along the pipe length for the base fluid and CuO-oil and CuO:MWCNT-oil nanofluids with different nanoparticle volume fractions at Re=750 are depicted in Fig. 5.20. As illustrated, Nusselt number is decreasing along the pipe length since the temperature difference between the wall surface and nanofluid mean temperature is minimum at the pipe inlet and increases along the pipe length. Moreover, the thermal boundary layer thickness is zero at the pipe entrance, and Nu is extremely large at $x = 0$. However, it decays rapidly as the thermal boundary layer develops.

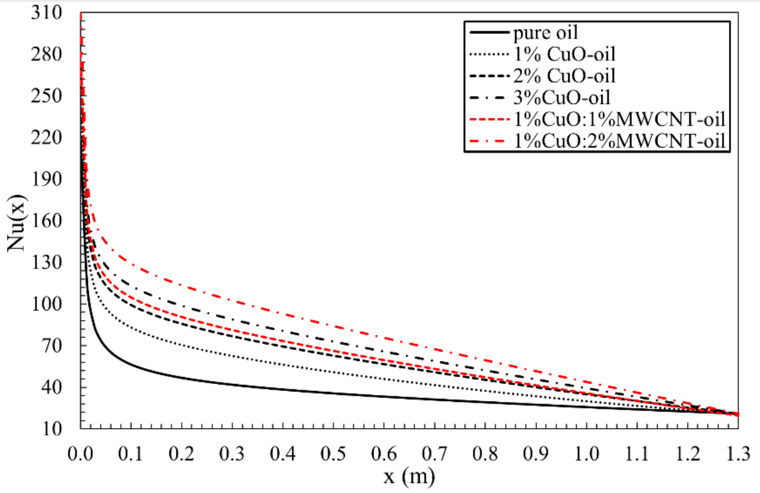

Fig. 5.20. Local Nusselt number along the pipe for different nanofluids at Re $= 750$.

The local Nusselt number for CuO-oil nanofluid shows an increasing trend with increasing nanoparticle volume fraction in the range of 0-3%. It proves that adding nanoparticles improved the oil's ability to transfer heat from the wall to the bulk of the nanofluid. Adding 3% of CuO can increase the average Nusselt number about 78%. Another important point is that 1%CuO:1%MWCNT-oil has higher Nusselt numbers in comparison with 2%CuO-oil although they have the same total nanoparticle volume fraction 2%. It can be concluded that adding MWCNT into the base fluid has more impact on improving heat transfer performance than adding CuO. The same conclusion can be drawn from the comparison between 3%CuO-oil and 1%CuO:2%MWCNT-oil.

Simulation results for the average heat transfer coefficient for different nanofluids with different volume fractions are presented in Table 5.1. The average heat transfer coefficient for nanofluids displays a rising trend as the nanoparticle volume fraction increases within the range of 0-3%. However, 1%CuO:1%MWCNT-oil has higher average heat transfer coefficient in comparison with 2%CuO-oil showing that MWCNT has more pronounced impact on improving heat transfer performance when compared to CuO. The comparison between 3% CuO-oil and 1% CuO:2% MWCNT-oil yields the same conclusion.

Table 5.1. Average heat transfer coefficient along the pipe for the base fluid and nanofluids at Re = 750.

Fluid	Average Heat Transfer Coefficient $\bar{h}$ (W/m^2K)
Engine oil (base fluid)	652.69
0.1%CuO-oil	746.36
0.2%CuO-oil	774.02
0.5%CuO-oil	833.16
1%CuO-oil	898.95
2%CuO-oil	1082.18
3%CuO-oil	1251.08
1%CuO:1%MWCNT-oil	1147.34
1%CuO:2%MWCNT-oil	1422.79

Figure 5.21 shows the influence of the CuO nanoparticle volume fraction on the Nusselt number along the 2D channel's lower wall for CuO-water nanofluid flow. As it is shown, when the volume fraction of CuO nanoparticles increases, the value of the Nusselt number along the bottom wall increases. It shows that nanoparticle volume fraction has an impact on Nusselt number along the channel. Nanofluid with 4% of nanoparticle concentration has the highest amount of Nusselt number along the channel.

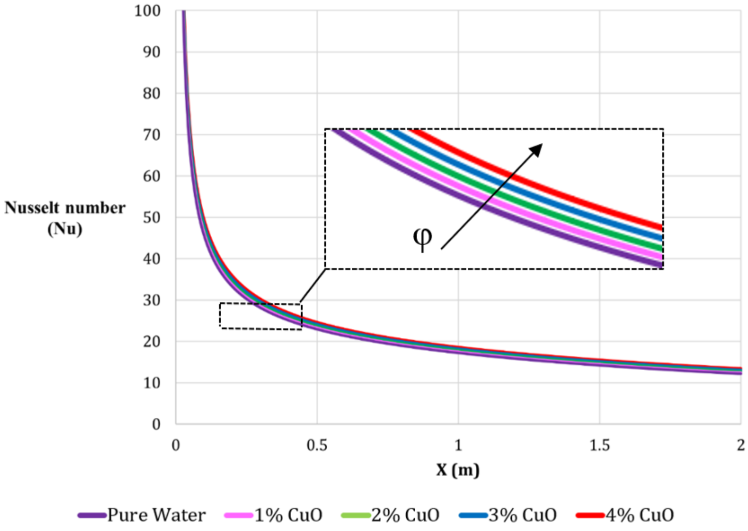

Fig. 5.21. Nusselt number at different volume fractions along the lower wall of pipe.

Numerical simulations on the 3D steady-state laminar flow of different water-based nanofluids in a horizontal pipe are conducted using the single-phase model considering temperature-dependent thermophysical properties. The simulations are performed to compare the heat transfer performance behavior for water-based nanofluids including Al_2O_3, CuO, TiO_2, and Ag nanoparticles under constant heat flux boundary condition on the pipe wall. Nanoparticle volume fractions ranging from 0.5% to 3% were examined at Reynolds numbers ranging from 310 to 1950.

Key parameters such as Nusselt number and heat transfer coefficient were analyzed. Figure 5.22 depicts the changes of average heat transfer coefficient for different nanofluids. The results show that Al_2O_3-water and Ag-water have the highest and the lowest heat transfer coefficient, respectively. Heat transfer coefficient increases with Reynolds number and volume fraction.

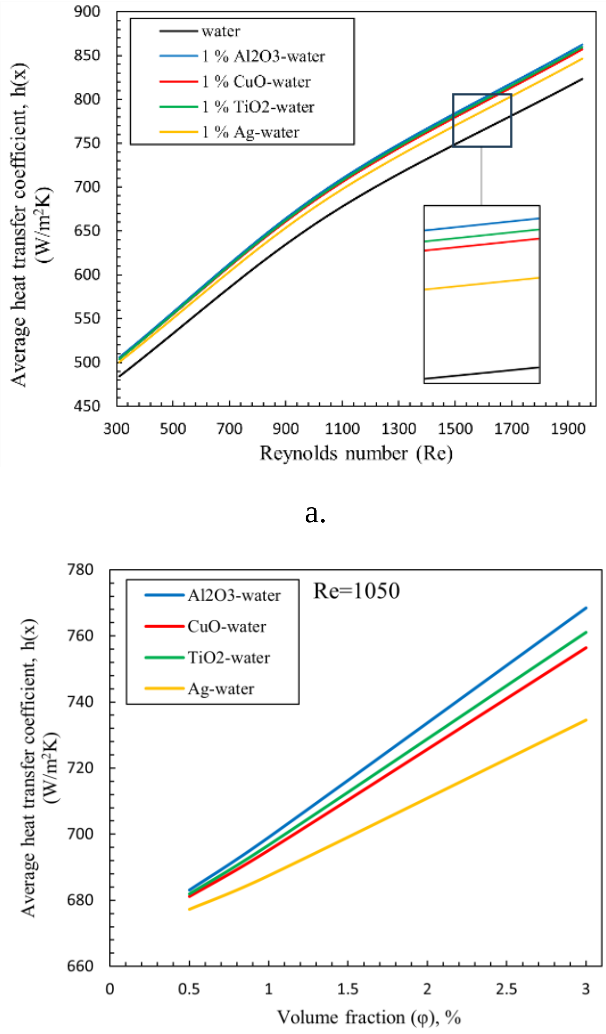

a.

b.

Fig. 5.22. Variation of the average heat transfer coefficient for different nanofluids: (a) at different Reynolds numbers, (b) at different volume fractions at Re=1050.

Figure 5.23 shows the changes of average Nusselt number for different nanofluids. The results show that TiO_2-water and Ag-water have the highest and the lowest Nusselt number, respectively. Nusselt number increases with increasing volume fraction for all nanofluids except for Ag-water nanofluid. This is due to the fact that Prandtl number for Ag-water nanofluid decreases with increasing volume fraction.

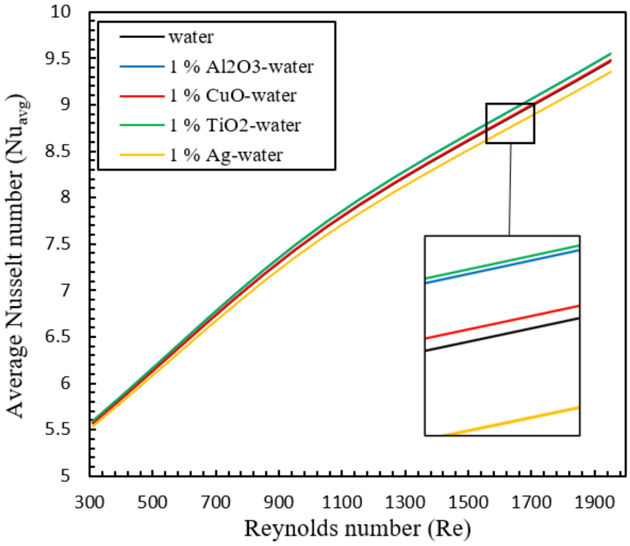

a.

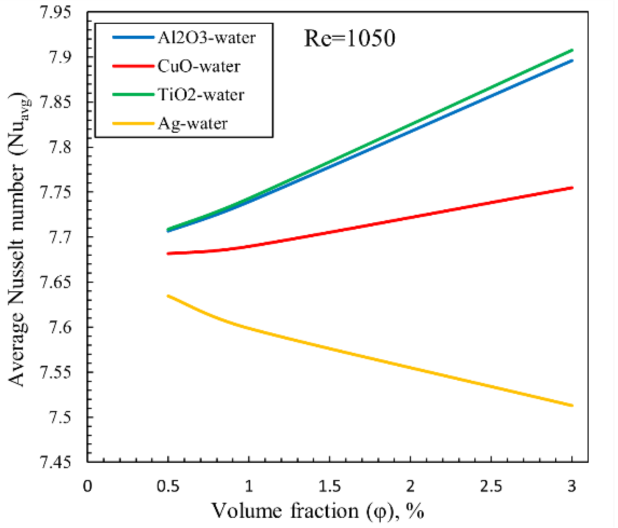

b.

Fig. 5.23. Variation of the Nusselt number for different nanofluids: (a) at volume fraction of 1% at different Reynolds numbers, (b) at different volume fractions at Re=1050.

5.6. HYDRODYNAMIC PERFORMANCE

This section presents the hydrodynamic performance of different nanofluids. Through detailed examination, it explores key factors such as Reynolds number, pressure drop, and pumping power, and wall shear stress and skin friction coefficient. By investigating these parameters and comparing the velocity contours and velocity profiles, it aims to provide insights into the fluid flow behavior and efficiency within the system.

5.6.1. REYNOLDS NUMBER, PRESSURE DROP, AND PUMPING POWER

Figure 5.24 illustrates the variation of the Reynolds number of the Al_2O_3-water nanofluid flow with volume fraction to obtain the same average heat transfer coefficient $h_{nf_{avg}} = 700\ W/m^2K$. The results show that the Reynolds number of the nanofluid flow decreases with increasing volume fraction to keep the average heat transfer coefficient constant.

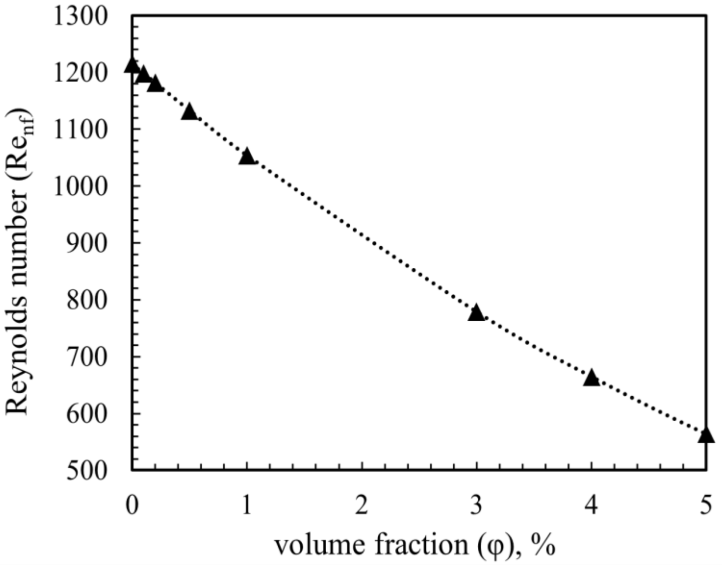

Fig. 5.24 Reynolds number versus volume fraction.

Figure 5.25 depicts the variation of the required pumping power of the Al_2O_3-water nanofluid flow with volume fraction to keep the average heat transfer coefficient constant at $h_{nf_{(avg)}} = 700\ W/m^2K$. It shows that the required pumping power decreases as the nanoparticle volume fraction for the nanofluid increases. Therefore, to obtain the same average heat transfer coefficient, lower pumping power is required compared to the base fluid.

Numerical simulations on the 3D steady-state laminar flow of different water-based nanofluids in a horizontal pipe are conducted using the single-phase model considering temperature-dependent thermophysical properties. The simulations are performed to compare the hydrodynamic behaviour for water-based nanofluids including Al_2O_3, CuO, TiO_2, and Ag nanoparticles under constant heat flux boundary condition on the pipe wall. Nanoparticle volume fractions ranging from 0.5% to 3% were examined at Reynolds numbers ranging from 310 to 1950. Key parameters such as pressure drop and pumping power were analysed. Figure 5.26 demonstrates the CFD results of the pumping power and the pressure drop for these water-based nanofluids at different Reynolds numbers. Al_2O_3-water and Ag-water have the highest and the lowest amount of pumping power and pressure drop, respectively.

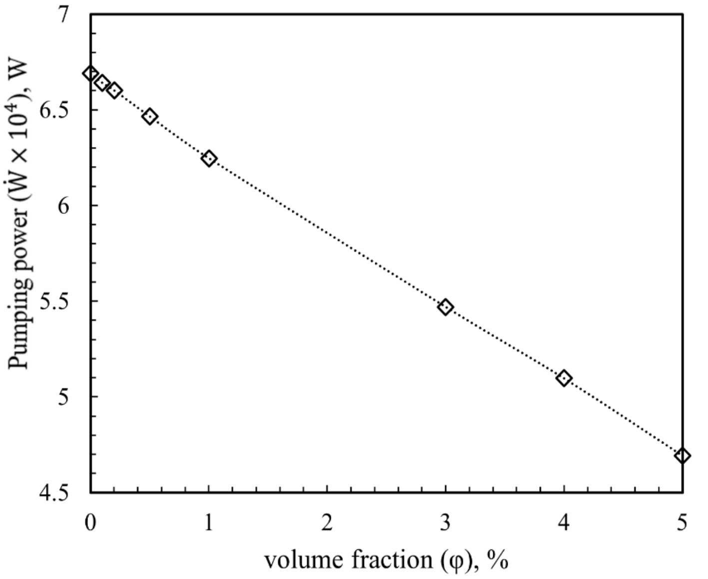

Fig. 5.25. Pumping power versus volume fraction.

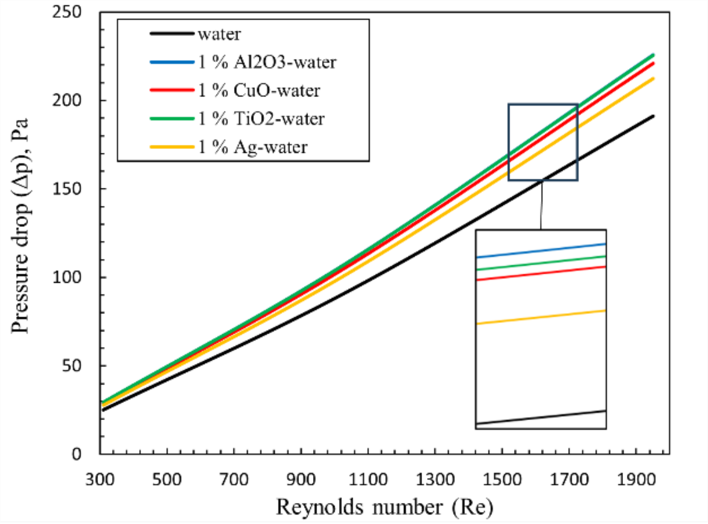

a

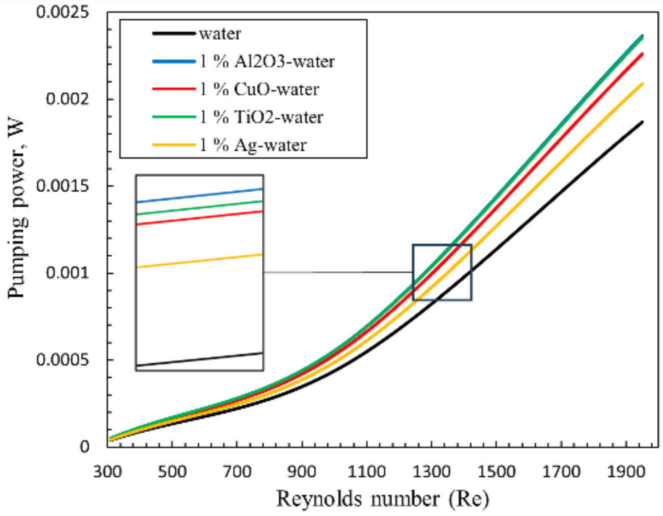

b.

Fig. 5.26. Variation of the pressure drop (a) and the pumping power (b) and with Reynolds number for different nanofluids at volume fraction of 1%.

5.6.2. VELOCITY CONTOUR

The velocity contour for CuO-water nanofluid containing 4% CuO along the section of the 2D channel which a fully developed regime was established is presented in Fig. 5.27. As it is illustrated, the velocity of nanofluid is not influenced by the thermal conditions at lower and upper walls, and it is only affected by the nanoparticle volume fraction. It is shown that the velocity near the walls is equal to zero due to no slip condition between walls and nanofluid. The velocity distribution along the channel is worthwhile to be studied. Therefore, two cross sections along the channel (X=0.1 and 0.5 m) are selected.

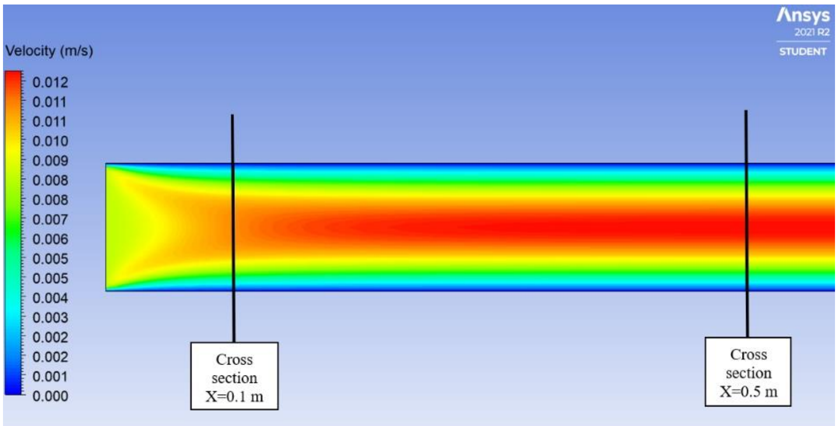

Fig. 5.27. Velocity contour for nanofluid containing 4% CuO along the pipe.

5.6.3. VELOCITY PROFILES

The velocity distributions of CuO-water nanofluid for nanoparticle volume fractions φ=1, 2, 3, and 4% of CuO with the inlet Reynold's number Re=1000 at cross sections X=0.1m and X=0.5 m along the 2D channel are shown in Figs. (5.28)-(5.29). The numerical simulations reveal that when the volume fraction increases, the velocity of nanofluid increases. Therefore, the volume fraction has an impact on the nanofluid's velocity, as shown by the results. It is shown that the maximum velocity of nanofluid happens at nanoparticle volume fraction equal to 4%. It can be observed from Fig. 5.28 that the velocity profile at cross section X=0.1 has not arrived the fully developed regime yet; however, there is a fully developed regime at cross section X=0.5 in Fig. 5.29.

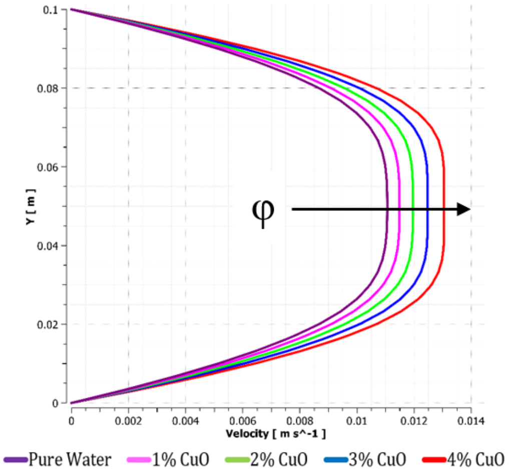

Fig. 5.28 Velocity distribution for different nanoparticle volume fractions at cross section X=0.1 m.

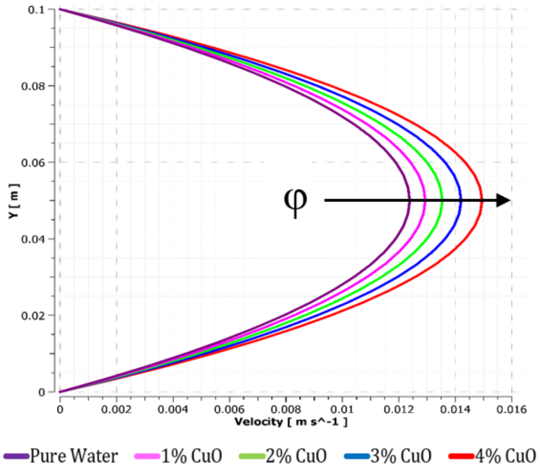

Fig. 5.29 Velocity distribution for different nanoparticle volume fractions at cross section X=0.5 m

.

Velocity profiles for CuO-oil and CuO:MWCNT-oil nanofluids with different nanoparticle volume fractions at three cross sectional areas along the pipe are depicted in Figs. (5.30)-(5.32). As illustrated, the velocity profiles for CuO-oil nanofluids show a decline with increasing nanoparticle concentration. It is due to the fact that at the same Reynolds numbers, the velocity values are directly proportional to the kinematic viscosity values of the fluid. On the other hand, as the nanoparticle volume fraction increases, the kinematic viscosity decreases for CuO-oil nanofluid (see Table 5.2). Hence, it is expected that velocity values for CuO-oil nanofluids show a decreasing trend with increasing nanoparticle volume fraction. However, 1%CuO:1%MWCNT-oil hybrid nanofluid and 1%CuO:2%MWCNT-oil hybrid nanofluid have higher kinematic viscosity values compared to 1%CuO-oil mono nanofluid, 2%CuO-oil mono nanofluid or 3%CuO-oil mono nanofluid, which implies that 1%CuO:1%MWCNT-oil hybrid nanofluid and 1%CuO:2%MWCNT-oil hybrid nanofluid have higher velocity values.

Table 5.2. Kinematic viscosity for the base fluid and nanofluids at *T*=45℃.

Fluid	Kinematic viscosity ($m^2/s\times10^6$)
Engine oil (base fluid)	28.79
0.1%CuO-oil	28.67
0.2%CuO-oil	28.56
0.5%CuO-oil	28.23
1%CuO-oil	27.71
2%CuO-oil	26.79
3%CuO-oil	26.00
1%CuO:1%MWCNT-oil	28.05
1%CuO:2%MWCNT-oil	28.41

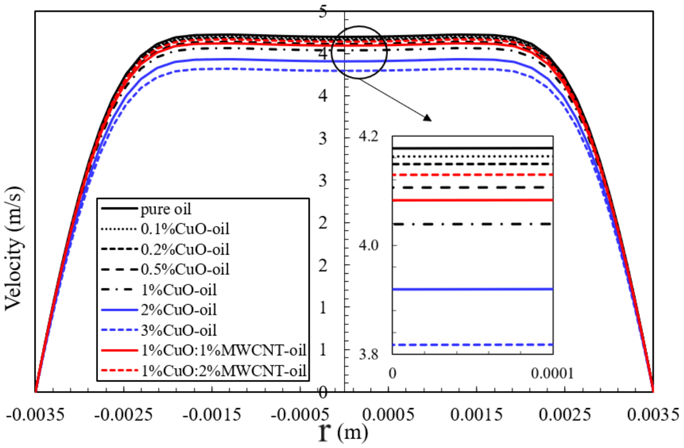

Fig. 5.30. Velocity profiles for the base fluid and nanofluids at *x*=0.02m.

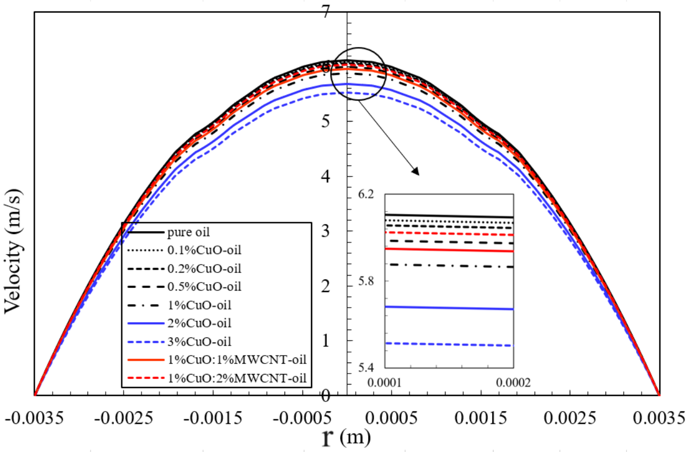

Fig. 5.31. Velocity profiles for the base fluid and nanofluids at *x*=0.65m.

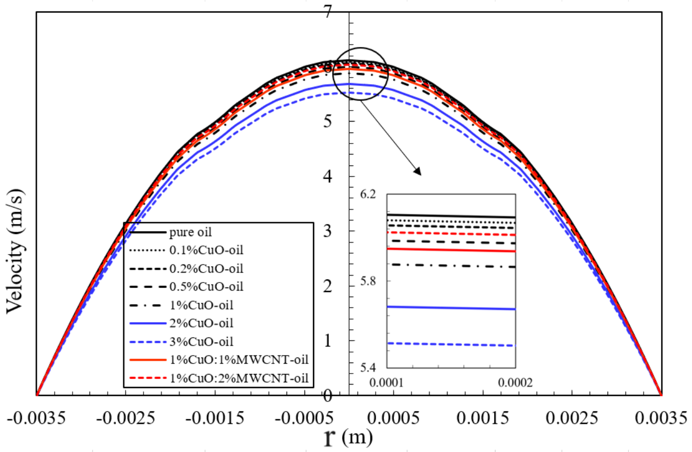

Fig. 5.32. Velocity profiles for the base fluid and nanofluids at *x*=1.3m.

Note that the velocity profiles presented in Figs. (5.31) and (5.32) are identical since both velocity profiles are located in the hydrodynamically (or velocity) fully developed region, where velocity profiles stop changing as the axial distance 'x' increases.

5.6.4. WALL SHEAR STRESS AND SKIN FRICTION COEFFICIENT

The wall shear stress and skin friction coefficient are both of engineering importance and will be shown and examined in detail. Figure 5.33 shows the influence of the CuO nanoparticle volume fraction on the wall shear stress along the 2D channel's lower wall for the CuO-water nanofluid flow. As it is shown, when the volume fraction of CuO nanoparticles increases, the value of the wall shear stress along the bottom wall increases. It shows that nanoparticle volume fraction has an impact on wall shear stress along the channel. Nanofluid with 4% nanoparticle concentration has the highest amount of wall shear stress along the channel.

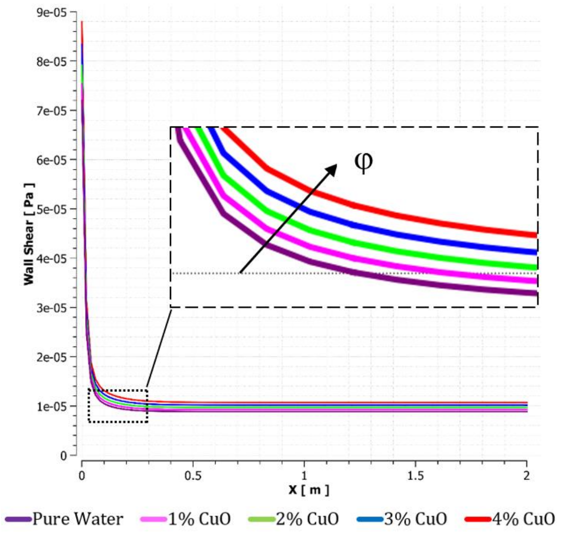

Fig. 5.33. Wall shear stress at different volume fractions along the lower wall of the pipe.

Figure 5.34 depicts the influence of the volume fraction on the skin friction coefficient along the channel's lower wall. As it is shown, when the volume fraction of CuO nanoparticles increases, the value of the skin friction coefficient along the bottom wall increases. It shows that nanoparticle volume fraction has an impact on skin friction coefficient along the channel. Nanofluid with 4% nanoparticle concentration has the highest amount of skin friction coefficient along the channel.

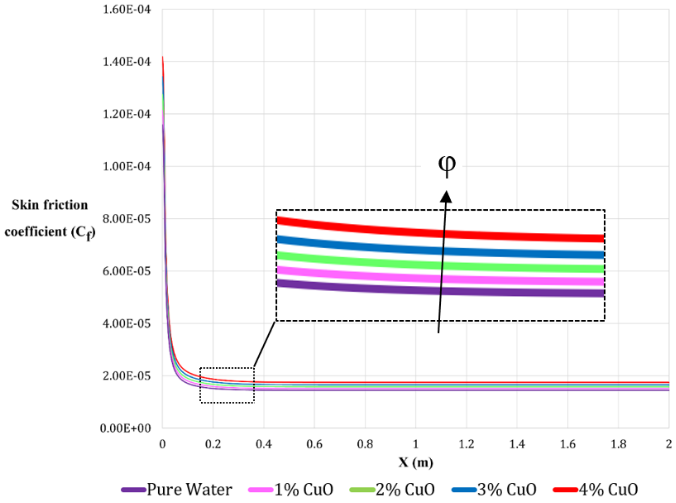

Fig. 5.34. The skin friction coefficient at different volume fractions along the lower wall of pipe.

5.7. THERMAL BOUNDARY LAYER THICKNESS AND SCALE ANALYSIS

Figure 5.35 displays the thermal boundary layer thickness δ_t along the pipe for the base fluid (oil) and CuO-oil and CuO:MWCNT-oil nanofluids with different volume fractions. As illustrated, the thickness of the thermal boundary layer grows as the distance from the entrance of the pipe increases. Another noteworthy observation is that the thickness of the thermal boundary layer for CuO-oil nanofluid increases as the nanoparticle concentration increases. However, 1%CuO:1%MWCNT-oil hybrid nanofluid and 1%CuO:2%MWCNT-oil hybrid nanofluid have smaller thermal boundary layer thickness in comparison with 2%CuO-oil nanofluid and 3%CuO-oil nanofluid, respectively. The main reason is that 1%CuO:1%MWCNT-oil hybrid nanofluid and 1%CuO:2%MWCNT-oil hybrid nanofluid have higher Prandtl number $\mathrm{Pr}_{nf} = \mu_{nf} C_{P_{nf}} / k_{nf}$ (see Table 5.3) and consequently, lower thermal diffusivity than 2%CuO-oil nanofluid and 3%CuO-oil nanofluid, respectively, which results in less energy being transported by diffusion within the thermal boundary layer region and having thinner thermal boundary layer thickness.

The values of average thermal boundary layer thickness for the base fluid and nanofluids with different concentrations are presented in Table 5.3.

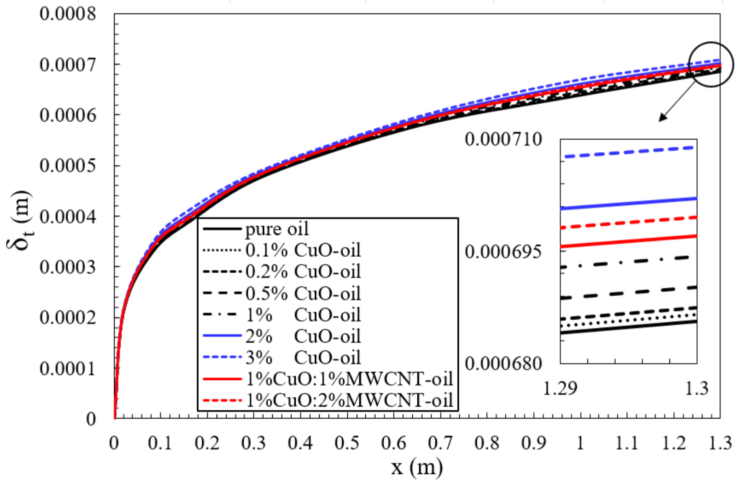

Fig. 5.35. Thermal boundary layer along the pipe for the base fluid and nanofluids at Re=750.

Table 5.3. Prandtl number T=45 ˚C and average thermal boundary layer thickness for the base fluid and nanofluids.

Fluid	Prandtl number, Pr	$\overline{\delta_t}, m$
Engine oil (base fluid)	397.08	0.000475
0.1%CuO-oil	394.72	0.000476
0.2%CuO-oil	392.38	0.000477
0.5%CuO-oil	385.58	0.000479
1%CuO-oil	374.87	0.000482
2%CuO-oil	355.50	0.000487
3%CuO-oil	338.49	0.000492
1%CuO:1%MWCNT-oil	368.04	0.000484
1%CuO:2%MWCNT-oil	361.73	0.000485

Scaling, also known as scale analysis, is a viable and inexpensive approach that offers order-of-magnitude estimations for quantities of concern using the fundamental concepts of engineering fields such as heat transfer, which can make it simpler to comprehend what the numerical findings are trying to tell us [69]. Scale analysis is performed to provide the degree of magnitude of the boundary layer thickness and more importantly the heat transfer coefficient. There is a no-slip condition at the surface, indicating that the fluid layer is attached to the pipe wall at r=R and it is stationary. Hence, heat is initially transferred from the pipe wall to the body of fluid inside the pipe by pure conduction. The local heat flux at any given axial pipe length 'x' may be obtained by utilizing Fourier's law on the fluid layer at the surface as

$$q'' = -k_{nf} \left. \frac{\partial T(x,r)}{\partial r} \right|_{r=R} . \tag{5.11}$$

Combining equations (4.5) and (5.11), the new expression for the local heat transfer coefficient at any given axial pipe length 'x' may be obtained as

$$h(x) = \frac{-k_{nf}\frac{\partial T(x,r)}{\partial r}\Big|_{r=R}}{T_s(x) - T_m(x)} . \tag{5.12}$$

The scale analysis of this equation yields

$$h(x) \sim \frac{k_{nf}(\Delta T/\delta_t(x))}{\Delta T} \sim \frac{k_{nf}}{\delta_t(x)} . \tag{5.13}$$

Putting scale relationships $h(x) \sim \bar{h}$ and $\delta_t(x) \sim \overline{\delta_t}$ into the above relationship (5.13) yields

$$\bar{h} \sim \frac{k_{nf}}{\overline{\delta_t}} . \tag{5.14}$$

This scaling analysis shows that the heat transfer coefficient is not just influenced by the thickness of the thermal boundary layer, but also by the thermal conductivity of the nanofluid. For instance, a rise in the thermal boundary layer thickness does not necessarily result in a decrease of the heat transfer coefficient. This may be observed by comparing $\bar{h}$ and $\overline{\delta_t}$values presented in Tables 5.1 and 5.3, where both exhibit an increasing trend with increasing volume fraction for the CuO-oil nanofluid. Therefore, another decisive factor is thermal conductivity which increases with increasing volume fraction for the CuO-oil nanofluid. Indeed, the ratio of $k_{nf}/\overline{\delta_t}$ tells us the degree of heat transfer coefficient's magnitude. In Table 5.4, values of $\mathrm{k_{nf}}/\overline{\delta_\mathrm{t}}$ calculated from the simulation results for all examined nanofluids are demonstrated. The degree of magnitude of these values is the same as the degree of magnitude of $\bar{h}$ values presented in Table 5.1. It reveals that the simulation results for the average heat transfer coefficient and the results of scale analysis calculated by relationship (5.14) are perfectly consistent.

Table 5.4. Scale analysis results $k_{nf}/\overline{\delta_t}$ for the base fluid and nanofluids at Re=750.

Fluid	$k_{nf}/\overline{\delta_t}$ (W/m^2K)
Engine oil (base fluid)	252.37
0.1%CuO-oil	255.76
0.2%CuO-oil	256.16
0.5%CuO-oil	257.40
1%CuO-oil	259.57
2%CuO-oil	264.25
3%CuO-oil	269.30
1%CuO:1%MWCNT-oil	266.31
1%CuO:2%MWCNT-oil	273.19

The scale analysis of the thickness of thermal boundary layer is performed for oil-based nanofluids which possess high Prandtl numbers, as follows [4]

$$\overline{\delta_t} \sim \mathrm{Pr}^{-1/2}\mathrm{Re}^{-1/2} . \tag{5.15}$$

The values of $\mathrm{Pr}^{-1/2}\mathrm{Re}^{-1/2}$ for all examined nanofluids are depicted in Table 5.5. The order of magnitude of these values is the same as the order of magnitude of simulation results of $\overline{\delta_t}$ presented in Table 5.3. It confirms that the simulation results of the average thickness for the thermal boundary layer perfectly agree with the scale analysis results calculated by relationship (5.15).

Table 5.5. Scale analysis results $\mathrm{Pr}^{-1/2}\mathrm{Re}^{-1/2}$ for the base fluid and nanofluids at Re=750.

Fluid	$\mathrm{Pr}^{-1/2}\mathrm{Re}^{-1/2}$
Engine oil (base fluid)	0.001832
0.1%CuO-oil	0.001838
0.2%CuO-oil	0.001843
0.5%CuO-oil	0.001860
1%CuO-oil	0.001886
2%CuO-oil	0.001937
3%CuO-oil	0.001985
1%CuO:1%MWCNT-oil	0.001903
1%CuO:2%MWCNT-oil	0.001920

Scale analysis was performed to provide the degree of magnitude of the boundary layer thickness and more importantly the heat transfer coefficient for mono CuO-oil nanofluid and hybrid CuO: MWCNT-oil nanofluid. It revealed that the simulation results for the boundary layer thickness as well as the average heat transfer coefficient are perfectly consistent with the results of scale analysis. CFD simulations showed that the thermal boundary layer thickness increases with increasing nanoparticle volume fraction. However, 1%CuO:1%MWCNT-oil and 1%CuO:2%MWCNT-oil showed lower thermal boundary layer thickness in comparison with their corresponding 2%CuO-oil and 3%CuO-oil because 1%CuO:1%MWCNT-oil and 1%CuO:2%MWCNT-oil have higher Prandtl numbers than 2%CuO-oil and 3%CuO-oil, and lower thermal diffusivity, so they have thinner thermal boundary layer thickness, too.

5.8. PERFORMANCE EFFICIENCY INDEX (PEI)

In Fig. 5.36, the performance efficiency index is depicted for Al_2O_3-water nanofluid with volume fractions ranging from 0.1% to 5% and Re between 650 and 1350. The graph reveals that the performance index is advantageous for nanofluids with a volume fraction under 1%.

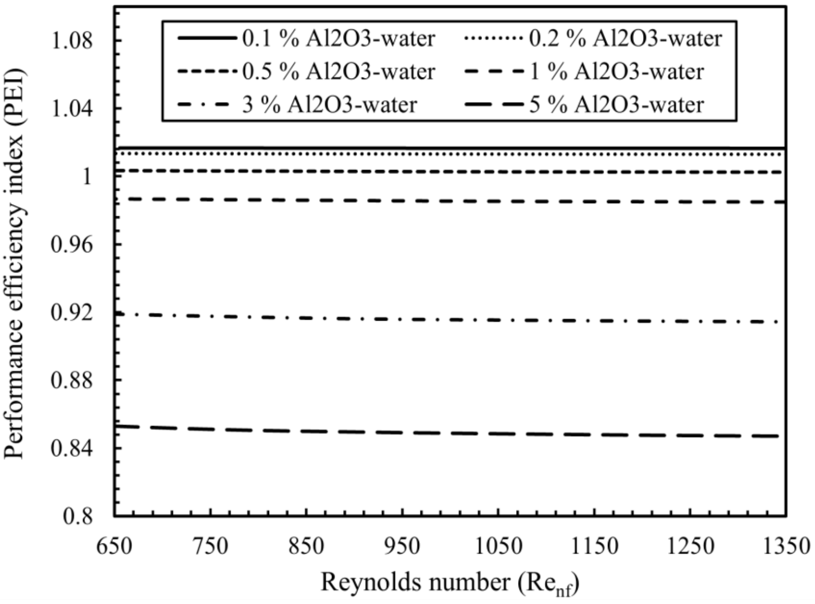

Fig. 5.36. PEI versus Reynolds number.

Figure 5.37 depicts the relationship between the performance efficiency index for Al_2O_3-water nanofluid and nanoparticle volume fraction within the range of 0.01% to 5% for two distinct inlet velocities: 0.09 m/s and 0.25 m/s. The results reveal that the performance efficiency index remains above one for volume fractions lower than 0.6%. The highest performance efficiency index is observed at the nanoparticle volume fraction of 0.1% for Al_2O_3-water nanofluid.

The influence of the heat transfer enhancement is more significant for smaller volume fractions (less than 0.1%) while for greater volume fractions the effect of the increasing friction factor is so noticeable that the performance efficiency index (PEI) even starts to decrease with increasing volume fraction more than 0.1%. This is due to the fact that the performance efficiency of nanofluids depends upon the ratio of heat transfer enhancement and pressure drop. The introduction of nanoparticles to the base fluid results in heightened thermal conductivity and increased Heat Transfer Coefficient (HTC). However, the elevated density of nanoparticles relative to the base fluid contributes to an augmented pressure drop. Consequently, the cumulative impact of nanoparticle incorporation into the base fluid leads to a decrease in the overall performance efficiency.

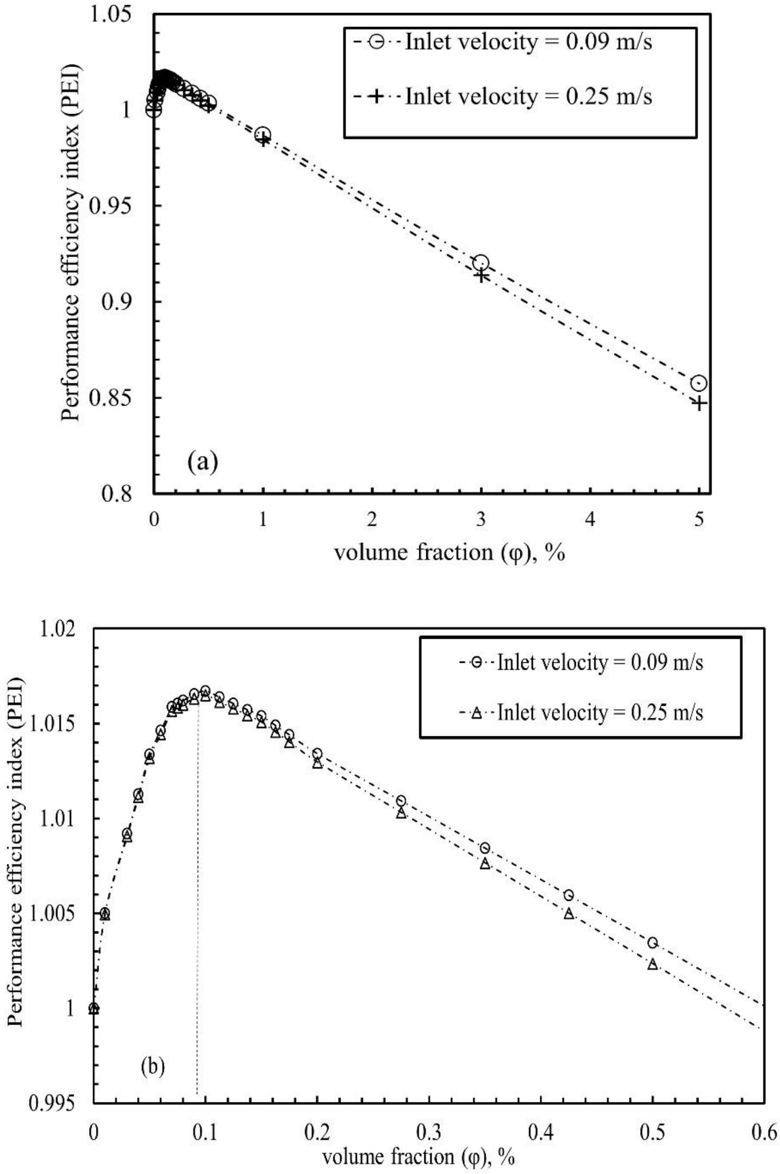

Fig. 5.37 Variation of the performance efficiency index for Al_2O_3-water nanofluid with nanoparticle volume fraction: $(a)\ 0\% < \varphi < 5\%$ (b) $0\% < \varphi < 0.6\%$.

6. NEW SCIENTIFIC RESULTS OF THE THESES

The main contributions from the research can be summarised as follows:

TH1. On the base of three-dimensional CFD simulations for Al_2O_3-water nanofluid of volume fractions ranging from 0.1% to 5% and using the notation

$$\mathrm{Re}_{nf} = \mathrm{Re}_{bf}\left(\frac{\rho_{nf}}{\rho_{bf}}\frac{\mu_{bf}}{\mu_{nf}}\right),$$

I determined the laminar hydrodynamic entry length as

$$X_{hy_{(nf)}} = 0.0554\,\mathrm{Re}_{nf}\,D_{in} = 0.0554\,\mathrm{Re}_{bf}\,A(\varphi,T)\,D_{in},$$

$$A(\varphi,T) = \frac{1+(a-1)\varphi}{1+9.4974\varphi+77.811\varphi^2+0.9514\varphi^3},$$

with $a(\varphi,T) = \frac{\rho_{np}}{\rho_{bf}}$, and also, the laminar thermal entry length of the nanofluid flow in a pipe as

$$X_{th_{(nf)}} = \left(0.043 - \frac{4.823\varphi}{10^6}\right)\mathrm{Re}_{nf}\mathrm{Pr}_{nf}D_{in} = \left(0.043 - \frac{4.823\varphi}{10^6}\right)\mathrm{A}(\varphi,T)\mathrm{B}(\varphi,T)\mathrm{Re}_{bf}\mathrm{Pr}_{bf}D_{in},$$

$$\mathrm{B}(\varphi,T) = (1+9.4974\varphi+77.811\varphi^2+0.9514\varphi^3)\,\frac{\frac{1-\varphi}{1-\varphi+a\varphi}+ab\varphi}{1+\frac{3(c-1)\beta^3\varphi}{c+2-(c-1)\beta^3\varphi}},$$

with $b(\varphi,T) = \frac{c_{p_{np}}}{c_{p_{bf}}}$, $c(\varphi,T)=\frac{k_{np}}{k_{bf}}$ [P1].

TH2. Experimental and theoretical investigations were published by Churchill-Ozoe [68], (5.4), and Shah-Grigull and they gave correlations [3,67], (5.1-5.3), for $\mathrm{Nu}(x)$ of base fluids. Moreover, experimental results were given by Esmaeilzadeh et al. [62] for Al_2O_3-water nanofluids. I performed simulations for three-dimensional steady-state flow of Al_2O_3-water nanofluid in a horizontal pipe with convective heat transfer on the wall when the thermophysical properties of the nanofluid are either constant or temperature-dependent. I showed that the numerical results agree well with Churchill-Ozoe correlation for temperature-dependent case and the Shah-Grigull correlations for the constant variables. My CFD results using temperature-dependent properties approximate Esmaeilzadeh's experimental data, with an average error of 2.44% for temperature-dependent case, but for the constant thermophysical properties I got a higher average error of 4.44%. These results suggest that considering temperature-dependent thermophysical properties can significantly improve the accuracy of simulations [P1].

TH3. Three-dimensional numerical simulations were conducted using Newtonian single-phase model for CuO-oil nanofluid flow in a pipe with nanoparticle volume fractions ranging from 0.1 to 3%. The results of my analysis indicated that increasing the nanoparticle concentration resulted in an increase in heat transfer. The incorporation of CuO nanoparticles in the base fluid at a volume concentration of 0.1% resulted in a 14% increase in heat transfer. The maximum improvement in heat transfer, which was 90%, was observed at the highest nanoparticle concentration of 3% volume. Furthermore, a rising trend in the local heat transfer coefficient was observed as the volume fraction of nanoparticles in the CuO-oil nanofluid increased within the range of 0-3%. The thickness of the thermal boundary layer was observed to increase with the nanoparticle concentration. This was due to the decrease in the Prandtl number resulting from the addition of nanoparticles, which led to a higher thermal diffusivity. Therefore, more energy was transported by diffusion within the thermal boundary layer region, resulting in a thicker thermal boundary layer when nanoparticles were added [P3]. CuO-water nanofluid flow within a horizontal 2D channel was also numerically investigated using CFD simulation. The maximum velocity shows an increase with increasing volume fraction. It is obtained that the temperature increased with increasing the volume fraction of CuO everywhere along the channel. Moreover, it is observed that when the volume fraction increases, the wall shear stress and skin friction coefficient, and Nusselt number along the channel increase as well [P4, P5].

TH4. Three-dimensional numerical simulations were conducted using Newtonian single-phase model for three different types of nanofluids including CuO-oil, CuO:MWCNT-oil 1:1, and CuO:MWCNT-oil 1:2 with different nanoparticle volume fractions ranging from 0.1 to 3%. Introduction of CuO nanoparticles in the base fluid as low as 0.1%vol can increase the heat transfer by 14%, with the highest particle loading (3%vol) producing a 78% enhancement in heat transfer. The heat transfer enhancement was more significant when applying hybrid nanofluid CuO:MWCNT-oil. Scale analysis was performed to provide the degree of magnitude of the boundary layer thickness and more importantly the heat transfer coefficient for mono CuO-oil nanofluid and hybrid CuO:MWCNT-oil nanofluid. It revealed that the simulation results for the boundary layer thickness as well as the average heat transfer coefficient are perfectly consistent with the results of scale analysis. CFD simulations showed that the thermal boundary layer thickness increases with increasing nanoparticle volume fraction. However, 1%CuO:1%MWCNT-oil and 1%CuO:2%MWCNT-oil showed thinner thermal boundary layer thickness in comparison with their corresponding 2%CuO-oil and 3%CuO-oil because 1%CuO:1%MWCNT-oil and 1%CuO:2%MWCNT-oil have higher Prandtl numbers (lower thermal diffusivity) than 2%CuO-oil and 3%CuO-oil, respectively [P6].

ACKNOWLEDGEMENTS

I would like to thank my PhD supervisors, **Prof. Dr. Gabriella Vadászné Bognár** and **Dr. Krisztián Hriczó**. Their constant support, guidance, and encouragement have been invaluable throughout the entire process. From the initial stages of refining my research proposal to the final submission of my thesis, their unwavering presence and wealth of wisdom have been instrumental in shaping my academic growth. I highly valued the biweekly meetings we held, which not only served as crucial checkpoints to keep me on track academically, but also provided me with plenty of encouragement. I am profoundly grateful for the immeasurable contributions they made to my development.

Mohsen Khalili Najafabadi

2024

REFERENCES

[1] Choi SUS. Enhancing thermal conductivity of fluids with nanoparticles. American Society of Mechanical Engineers, Fluids Engineering Division (Publication) FED 1995;231:99–105.

[2] Das SK, Putra N, Thiesen P, Roetzel W. Temperature dependence of thermal conductivity enhancement for nanofluids. Journal of Heat Transfer 2003;125:567–74. https://doi.org/10.1115/1.1571080.

[3] R. K. Shah, A. L. London. Laminar Flow Forced Convection in Ducts: A Source Book for Compact Heat Exchanger Analytical Data. New York: ACADEMIC PRESS, INC.; 1978.

[4] Adrian B. Convection Heat Transfer. 4th ed. Hoboken, New Jersey: John Wiley & Sons, Inc.; 2013.

[5] Yang Y, Zhang ZG, Grulke EA, Anderson WB, Wu G. Heat transfer properties of nanoparticle-in-fluid dispersions (nanofluids) in laminar flow. International Journal of Heat and Mass Transfer 2005;48:1107–16. https://doi.org/10.1016/j.ijheatmasstransfer.2004.09.038.

[6] Xiong Q, Hajjar A, Alshuraiaan B, Izadi M, Altnji S, Shehzad SA. State-of-the-art review of nanofluids in solar collectors: A review based on the type of the dispersed nanoparticles. Journal of Cleaner Production 2021;310:127528. https://doi.org/10.1016/j.jclepro.2021.127528.

[7] Mahian O, Kianifar A, Sahin AZ, Wongwises S. Performance analysis of a minichannel-based solar collector using different nanofluids. Energy Conversion and Management 2014;88:129–38. https://doi.org/10.1016/j.enconman.2014.08.021.

[8] Hwang KS, Jang SP, Choi SUS. Flow and convective heat transfer characteristics of water-based Al2O3 nanofluids in fully developed laminar flow regime. International Journal of Heat and Mass Transfer 2009;52:193–9. https://doi.org/10.1016/j.ijheatmasstransfer.2008.06.032.

[9] Huang D, Wu Z, Sunden B. Pressure drop and convective heat transfer of Al2O3/water and MWCNT/water nanofluids in a chevron plate heat exchanger. International Journal of Heat and Mass Transfer 2015;89:620–6. https://doi.org/10.1016/j.ijheatmasstransfer.2015.05.082.

[10] Alim MA, Abdin Z, Saidur R, Hepbasli A, Khairul MA, Rahim NA. Analyses of entropy generation and pressure drop for a conventional flat plate solar collector using different types of metal oxide nanofluids. Energy and Buildings 2013;66:289–96. https://doi.org/10.1016/j.enbuild.2013.07.027.

[11] Yousefi T, Veysi F, Shojaeizadeh E, Zinadini S. An experimental investigation on the effect of Al2O3-H2O nanofluid on the efficiency of flat-plate solar collectors. Renewable Energy 2012;39:293–8. https://doi.org/10.1016/j.renene.2011.08.056.

[12] Asadi A, Pourfattah F. Heat transfer performance of two oil-based nanofluids containing ZnO and MgO nanoparticles; a comparative experimental investigation. Powder Technology 2019;343:296–308. https://doi.org/10.1016/j.powtec.2018.11.023.

[13] Asadi A, Aberoumand S, Moradikazerouni A, Pourfattah F, Żyła G, Estellé P, et al. Recent advances in preparation methods and thermophysical properties of oil-based

nanofluids: A state-of-the-art review. Powder Technology 2019;352:209–26. https://doi.org/10.1016/j.powtec.2019.04.054.

[14] Li W, Zou C, Li X. Thermo-physical properties of waste cooking oil-based nanofluids. Applied Thermal Engineering 2017;112:784–92. https://doi.org/10.1016/J.APPLTHERMALENG.2016.10.136.

[15] Kole M, Dey TK. Enhanced thermophysical properties of copper nanoparticles dispersed in gear oil. Applied Thermal Engineering 2013;56:45–53. https://doi.org/10.1016/J.APPLTHERMALENG.2013.03.022.

[16] Beheshti A, Shanbedi M, Heris SZ. Heat transfer and rheological properties of transformer oil-oxidized MWCNT nanofluid. Journal of Thermal Analysis and Calorimetry 2014;118:1451–60. https://doi.org/10.1007/S10973-014-4048-0.

[17] Asadi M, Asadi A, Aberoumand S. An experimental and theoretical investigation on the effects of adding hybrid nanoparticles on heat transfer efficiency and pumping power of an oil-based nanofluid as a coolant fluid. International Journal of Refrigeration 2018;89:83–92. https://doi.org/10.1016/j.ijrefrig.2018.03.014.

[18] Mahamude ASF, Kamarulzaman MK, Harun WSW, Kadirgama K, Ramasamy D, Farhana K, et al. A Comprehensive Review on Efficiency Enhancement of Solar Collectors Using Hybrid Nanofluids. Energies 2022;15. https://doi.org/10.3390/en15041391.

[19] Che Sidik NA, Mahmud Jamil M, Aziz Japar WMA, Muhammad Adamu I. A review on preparation methods, stability and applications of hybrid nanofluids. Renewable and Sustainable Energy Reviews 2017;80:1112–22. https://doi.org/10.1016/J.RSER.2017.05.221.

[20] Sarkar J, Ghosh P, Adil A. A review on hybrid nanofluids: Recent research, development and applications. Renewable and Sustainable Energy Reviews 2015;43:164–77. https://doi.org/10.1016/J.RSER.2014.11.023.

[21] Benkhedda M, Boufendi T, Touahri S, Benkhedda M, Boufendi T, Touahri S. Laminar mixed convective heat transfer enhancement by using Ag-TiO₂-water hybrid Nanofluid in a heated horizontal annulus. HMT 2018;54:2799–814. https://doi.org/10.1007/S00231-018-2302-X.

[22] Rahman MRA, Leong KY, Idris AC, Saad MR, Anwar M. Numerical analysis of the forced convective heat transfer on Al2O3–Cu/water hybrid nanofluid. Heat and Mass Transfer 2017;5:1835–42. https://doi.org/10.1007/S00231-016-1941-Z.

[23] Vallejo JP, Prado JI, Lugo L. Hybrid or mono nanofluids for convective heat transfer applications. A critical review of experimental research. Applied Thermal Engineering 2022;203:117926. https://doi.org/10.1016/j.applthermaleng.2021.117926.

[24] Hemmat Esfe M, Afrand M, Gharehkhani S, Rostamian H, Toghraie D, Dahari M. An experimental study on viscosity of alumina-engine oil: Effects of temperature and nanoparticles concentration. International Communications in Heat and Mass Transfer 2016;C:202–8. https://doi.org/10.1016/J.ICHEATMASSTRANSFER.2016.05.013.

[25] Saeedinia M, Akhavan-Behabadi MA, Razi P. Thermal and rheological characteristics of CuO-Base oil nanofluid flow inside a circular tube. International Communications in Heat and Mass Transfer 2012;39:152–9. https://doi.org/10.1016/j.icheatmasstransfer.2011.08.001.

[26] Farbod M, Kouhpeymani R, Reza A. Morphology dependence of thermal and rheological properties of oil-based nanofluids of CuO nanostructures. Colloids and Surfaces A: Physicochemical and Engineering Aspects 2015;474:71–5. https://doi.org/10.1016/j.colsurfa.2015.02.049.

[27] Suresh S, Venkitaraj KP, Selvakumar P, Chandrasekar M. Effect of Al 2O 3-Cu/water hybrid nanofluid in heat transfer. Experimental Thermal and Fluid Science 2012;38:54–60. https://doi.org/10.1016/J.EXPTHERMFLUSCI.2011.11.007.

[28] Suresh S, Venkitaraj KP, Hameed MS, Sarangan J. Turbulent heat transfer and pressure drop characteristics of dilute water based Al2O3-Cu hybrid nanofluids 2014;14:2563–72. https://doi.org/10.1166/JNN.2014.8467.

[29] Kumar P, Sharma K V, Adriana A, Kesti V. International Journal of Thermal Sciences Experimental and computational determination of heat transfer , entropy generation and pressure drop under turbulent flow in a tube with fly ash-Cu hybrid nanofluid. International Journal of Thermal Sciences 2021;167:107016. https://doi.org/10.1016/j.ijthermalsci.2021.107016.

[30] Kanti P, Sharma K V., Said Z, Kesti V. Entropy generation and friction factor analysis of fly ash nanofluids flowing in a horizontal tube: Experimental and numerical study. International Journal of Thermal Sciences 2021;166:106972. https://doi.org/10.1016/J.IJTHERMALSCI.2021.106972.

[31] Kanti P, Sharma K V., Said Z, Bellos E. Numerical study on the thermo-hydraulic performance analysis of fly ash nanofluid. Journal of Thermal Analysis and Calorimetry 2022;147:2101–13. https://doi.org/10.1007/S10973-020-10533-0/METRICS.

[32] Pagliarini G. Steady laminar heat transfer in the entry region of circular tubes with axial diffusion of heat and momentum. International Journal of Heat and Mass Transfer 1989;32:1037–52. https://doi.org/10.1016/0017-9310(89)90005-7.

[33] Worsøe-Schmidt PM. Heat transfer in the thermal entrance region of circular tubes and annular passages with fully developed laminar flow. International Journal of Heat and Mass Transfer 1967;10:541–51. https://doi.org/10.1016/0017-9310(67)90173-1.

[34] Ma H, He B, Su L, He D. Heat transfer enhancement of nanofluid flow at the entry region of microtubes. International Journal of Thermal Sciences 2023;184. https://doi.org/10.1016/j.ijthermalsci.2022.107944.

[35] Çengel YA, Cimbala JM. Fluid Mechanics: Fundamentals and Applications. Third. New York: The McGraw-Hill Companies, Inc.; 2014.

[36] Everts M, Meyer JP. Laminar hydrodynamic and thermal entrance lengths for simultaneously hydrodynamically and thermally developing forced and mixed convective flows in horizontal tubes. Experimental Thermal and Fluid Science 2020;118:110153. https://doi.org/10.1016/j.expthermflusci.2020.110153.

[37] Atkinson B, Brocklebank MP, Card CCH, Smith JM. Low Reynolds number developing flows. AIChE Journal 1969;15:548–53. https://doi.org/10.1002/aic.690150414.

[38] Durst F, Ray S, Ünsal B, Bayoumi OA. The development lengths of laminar pipe and channel flows. Journal of Fluids Engineering, Transactions of the ASME 2005;127:1154–60. https://doi.org/10.1115/1.2063088.

[39] Joshi Y, Vinoth BR. Entry Lengths of Laminar Pipe and Channel Flows. Journal of Fluids Engineering, Transactions of the ASME 2018;140. https://doi.org/10.1115/1.4038668.

[40] Yunus A. Çengel, Afshin J. Ghajar. Heat And Mass Transfer: Fundamentals and Applications. Sixth. New York: McGraw-Hill Education; 2020.

[41] Nguyen T V. Incremental heat transfer number in the entry region of circular tubes. International Journal of Heat and Mass Transfer 1993;36:3659–62. https://doi.org/10.1016/0017-9310(93)90182-6.

[42] Zahmatkesh I, Sheremet M, Yang L, Heris SZ, Sharifpur M, Meyer JP, et al. Effect of nanoparticle shape on the performance of thermal systems utilizing nanofluids: A critical review. Journal of Molecular Liquids 2021;321. https://doi.org/10.1016/J.MOLLIQ.2020.114430.

[43] Liang G, Mudawar I. Review of single-phase and two-phase nanofluid heat transfer in macro-channels and micro-channels. International Journal of Heat and Mass Transfer 2019;136:324–54. https://doi.org/10.1016/j.ijheatmasstransfer.2019.02.086.

[44] Rashidi MM, Nazari MA, Mahariq I, Assad MEH, Ali ME, Almuzaiqer R, et al.

Thermophysical properties of hybrid nanofluids and the proposed models: An updated comprehensive study. Nanomaterials 2021;11. https://doi.org/10.3390/nano11113084.

[45] Alwan MS, Hadi JM, Jaafer LH, Jalghaf HK. Study the effect of nano fluid on heat transfer in finned pipe with internal v-cut twisted tape. Journal of Mechanical Engineering Research and Developments 2020;43:161–77.

[46] Minkowycz WJ, Sparrow EM, Abraham JP. Nanoparticle heat transfer and fluid flow. vol. 4. Boca Raton: Taylor & Francis; 2013. https://doi.org/10.1201/b12983.

[47] Klazly M, Bognár G. A novel empirical equation for the effective viscosity of nanofluids based on theoretical and empirical results. International Communications in Heat and Mass Transfer 2022;135:106054. https://doi.org/10.1016/j.icheatmasstransfer.2022.106054.

[48] Yu W, Choi SUS. The role of interfacial layers in the enhanced thermal conductivity of nanofluids: A renovated Maxwell model. Journal of Nanoparticle Research 2003;5:167–71. https://doi.org/10.1023/A:1024438603801/METRICS.

[49] Klazly M, Bognar G. Heat transfer enhancement for nanofluid flows over a microscale backward-facing step. Alexandria Engineering Journal 2022;61:8161–76. https://doi.org/10.1016/j.aej.2022.01.008.

[50] Mahbubul IM, Saidur R, Amalina MA. Latest developments on the viscosity of nanofluids. International Journal of Heat and Mass Transfer 2012;55:874–85. https://doi.org/10.1016/j.ijheatmasstransfer.2011.10.021.

[51] Abu-Nada E. Application of nanofluids for heat transfer enhancement of separated flows encountered in a backward facing step. International Journal of Heat and Fluid Flow 2008;29:242–9. https://doi.org/10.1016/j.ijheatfluidflow.2007.07.001.

[52] Kakaç S, Pramuanjaroenkij A. Review of convective heat transfer enhancement with nanofluids. International Journal of Heat and Mass Transfer 2009;52:3187–96. https://doi.org/10.1016/j.ijheatmasstransfer.2009.02.006.

[53] Kherbeet AS, Mohammed HA, Salman BH. International Journal of Heat and Mass Transfer The effect of nanofluids flow on mixed convection heat transfer over microscale backward-facing step. International Journal of Heat and Mass Transfer 2012;55:5870–81. https://doi.org/10.1016/j.ijheatmasstransfer.2012.05.084.

[54] Sajadi AR, Kazemi MH. Investigation of turbulent convective heat transfer and pressure drop of TiO2/water nanofluid in circular tube. International Communications in Heat and Mass Transfer 2011;38:1474–8. https://doi.org/10.1016/j.icheatmasstransfer.2011.07.007.

[55] Hayat T, Nadeem S. Heat transfer enhancement with Ag–CuO/water hybrid nanofluid. Results in Physics 2017;7:2317–24. https://doi.org/10.1016/j.rinp.2017.06.034.

[56] Fazeli I, Reza M, Emami S, Rashidi A. Investigation and optimization of the behavior of heat transfer and flow of MWCNT-CuO hybrid nanofluid in a brazed plate heat exchanger using response surface methodology. International Communications in Heat and Mass Transfer 2021;122:105175. https://doi.org/10.1016/j.icheatmasstransfer.2021.105175.

[57] Heris SZ, Farzin F, Sardarabadi H. Experimental Comparison Among Thermal Characteristics of Three Metal Oxide Nanoparticles/Turbine Oil-Based Nanofluids Under Laminar Flow Regime. International Journal of Thermophysics 2015;36:760–82. https://doi.org/10.1007/s10765-015-1852-0.

[58] Pak BC, Cho YI. Hydrodynamic and heat transfer study of dispersed fluids with submicron metallic oxide particles. Experimental Heat Transfer 1998;11:151–70. https://doi.org/10.1080/08916159808946559.

[59] Takabi B, Salehi S. Augmentation of the heat transfer performance of a sinusoidal corrugated enclosure by employing hybrid nanofluid. Advances in Mechanical Engineering 2014;2014. https://doi.org/10.1155/2014/147059.

[60] Hamilton RL. Thermal conductivity of heterogeneous two-component systems. Industrial

and Engineering Chemistry Fundamentals 1962;1:187–91. https://doi.org/10.1021/i160003a005.

[61] BATCHELOR GK. The effect of Brownian motion on the bulk stress in a suspension of spherical particles. Fluid Mech 1977;83:97–117.

[62] Esmaeilzadeh E, Almohammadi H, Nasiri Vatan S, Omrani AN. Experimental investigation of hydrodynamics and heat transfer characteristics of γ-Al2O3/water under laminar flow inside a horizontal tube. International Journal of Thermal Sciences 2013;63:31–7. https://doi.org/10.1016/j.ijthermalsci.2012.07.001.

[63] Klazly MM, Bognár G. CFD investigation of backward - Facing step nanofluid flow. Journal of Physics: Conference Series 2020;1564. https://doi.org/10.1088/1742-6596/1564/1/012010.

[64] Kanti PK, Sharma K V., Minea AA, Kesti V. Experimental and computational determination of heat transfer, entropy generation and pressure drop under turbulent flow in a tube with fly ash-Cu hybrid nanofluid. International Journal of Thermal Sciences 2021;167:107016. https://doi.org/10.1016/J.IJTHERMALSCI.2021.107016.

[65] Prasher R, Song D, Wang J, Phelan P. Measurements of nanofluid viscosity and its implications for thermal applications. Applied Physics Letters 2006;89:67–70. https://doi.org/10.1063/1.2356113.

[66] Bergman TL adrienne SL. Fundamentals of Heat and Mass Transfer. 8th ed. John Wiley & Sons, Ltd; 2017.

[67] Grigull U, Tratz H. Thermischer einlauf in ausgebildeter laminarer rohrströmung. International Journal of Heat and Mass Transfer 1965;8:669–78. https://doi.org/10.1016/0017-9310(65)90016-5.

[68] Churchill SW, Ozoe H. Correlations for laminar forced convection with uniform heating in flow over a plate and in developing and fully developed flow in a tube. Journal of Heat Transfer 1973;95:78–84. https://doi.org/10.1115/1.3450009.

[69] Faghri A, Zhang Y. Transport Phenomena in Multiphase Systems. 1st ed. Elsevier Inc; 2006.

LIST OF PUBLICATIONS RELATED TO THE TOPIC OF THE RESEARCH FIELD

[P1] M.Khalili, K.Hriczó, G.Bognár, *Entry length correlations for alumina-water nanofluid in laminar pipe flow,* INTERNATIONAL JOURNAL OF THERMAL SCIENCES (1290-0729 1778-4166): 197 Paper 108808. 10 p. (2024)

[P2] M.Khalili, M.Klazly, S.Okhunjon, , K.Hriczó, G.Bognár, *CFD study of heat transfer enhancement for* Al_2O_3*-turbine oil nanofluid flow in a pipe,* AIP CONFERENCE PROCEEDINGS (0094-243X 1551-7616): 2849 1 Paper 160006. 6 p. (2023)

[P3] M.Khalili, K.Hriczó, G.Bognár, *Thermal boundary layer analysis for CuO-engine oil laminar flow in a pipe,* Ankara: ACADEMY OF SCIENTIFIC AND EDUCATIONAL STUDIES, pp 211-217 (2023)

[P4] M.Khalili, K.Hriczó, G.Bognár, *Heat transfer characteristics of water-CuO nanofluid flow inside 2D pipe,* 8th International Scientific Conference on Advances in Mechanical Engineering (ISCAME 2022) : Conference proceedings, Debrecen, pp 52-53 (2022)

[P5] M.Khalili, K.Hriczó, G.Bognár, *The effects of water-CuO nanofluid flow on heat transfer inside a heated 2D channel,* DESIGN OF MACHINES AND STRUCTURES (1785-6892 2064-7522): 12 1 pp 47-62 (2022)

[P6] M.Khalili, K.Hriczó, G.Bognár, *Impact of CuO-MWCNT Nanoparticles on the Heat Transfer of Oil Nanofluid in a Pipe,* (Submitted)